Published in final edited form as:
Phys Chem Chem Phys. 2014 February 7; 16(5): 1759–1787. doi:10.1039/c3cp53413h.

Fully anharmonic IR and Raman spectra of medium-size molecular systems: accuracy and interpretation†

Vincenzo Barone[*,a], **Malgorzata Biczysko**[a], and **Julien Bloino**[a,b]

[a]Scuola Normale Superiore, piazza dei Cavalieri 7, I-56126 Pisa, Italy

[b]Consiglio Nazionale delle Ricerche, Istituto di Chimica dei Composti OrganoMetallici (ICCOM-CNR), UOS di Pisa, Area della Ricerca CNR, Via G. Moruzzi 1, I-56124 Pisa, Italy

Abstract

Computation of full infrared (IR) and Raman spectra (including absolute intensities and transition energies) for medium- and large-sized molecular systems beyond the harmonic approximation is one of the most interesting challenges of contemporary computational chemistry. Contrary to common beliefs, low-order perturbation theory is able to deliver results of high accuracy (actually often better than those issuing from current direct dynamics approaches) provided that anharmonic resonances are properly managed. This perspective sketches the recent developments in our research group toward the development a robust and user-friendly virtual spectrometer rooted into the second-order vibrational perturbation theory (VPT2) and usable also by non-specialists essentially as a black-box procedure. Several examples are explicitly worked out in order to illustrate the features of our computational tool together with the most important ongoing developments.

1 Introduction

Vibrational spectroscopy, in particular when combining different techniques (essentially IR and Raman) able to provide a detailed insight on the whole vibrational spectrum, is a very powerful tool for the investigation of structural and dynamical properties of any kind of molecular systems[1–4]. Nowadays, interpretation and analysis of the experimental spectroscopy outcome is rather routinely aided by quantum mechanical (QM) computations of increasing accuracy and effectiveness[5–14]. Together with vibrational energies, IR intensities and Raman activities convey further information about internal motions, but their computation requires the evaluation of transition matrix elements of dipole moment and polarizability, between the initial and final state (see for example Ref.[15]). Within the Born-Oppenheimer approximation the problem can be formally cast in terms of potential energy (PES)[16,17] and property (PS)[16,18,19] surfaces, which determine the overall spectroscopic outcome. Most of current computations for all but the smallest molecules[20–25] are performed

†Electronic Supplementary Information (ESI) available: (*i*) Basis sets from N07D/SNSD family. (*ii*) Best-estimated anharmonic vibrational frequencies and Raman activities for the six conformers of glycine, for all fundamental bands, overtones (2_i) and combination bands (1_i1_j). See DOI: 10.1039/b000000x/

*vincenzo.barone@sns.it.
malgorzata.biczysko@sns.it julien.bloino@pi.iccom.cnr.it

Europe PMC Funders Author Manuscripts

in the so-called double harmonic approximation in which the PES is truncated at the second order and the PS at the first order[15]. A common practice to improve the accuracy of those calculations is to resort to simple[26–31] or more sophisticated scaling methods[26,32,33] applied to harmonic wavenumbers in order to correct band positions of fundamental transitions. It should be noted that such methodologies based on the double-harmonic approximation do not provide any information about the intensities of overtones and combination bands, which might be necessary to correctly analyse experimental outcomes. For example, more refined computations are needed to distinguish low-intensity features related to non-fundamental transitions of the most populated species present in experimental mixtures from fundamental transitions of the less abundant species.

With the increase of computer performance, generally applicable methods going beyond the harmonic approximation to obtain reliable vibrational wavenumbers of medium-to-large size systems have gained considerable interest[3,4,34]. A possible strategy is to use dynamical (time-dependent) approaches[35–38], but, due to the current hardware limitations, the accuracy of the underlying electronic computations remains quite limited, and, at the same time use of classical mechanics for the integration of equations of motion is questionable especially for the gas phase spectra. In our opinion the claimed quantitative accuracy often results from an error compensation between the underestimation of anharmonic effects related to the use of classical dynamics and the contemporary underestimation of harmonic vibrational energies related to the use of conventional functionals. This is confirmed, for instance, by a recent paper by Kirchner and coworkers,[37] which shows a nearly perfect agreement between molecular dynamics and conventional harmonic results. Alternatively, several time-independent routes have been followed in order to provide robust approaches, going beyond ‘ad-hoc’ implementations for specific molecular systems. Within this frame the most effective implementations are, at present, rooted into the second-order vibrational perturbation theory (VPT2)[39–61] and vibrational self-consistent field (VSCF), possibly followed by perturbative or variational (VCI) treatments of phonon correlation[60,62–72]. In particular, the pioneering works on both VPT2 and VCI approaches by Handy and co-workers led to the developments and implementations widely used in the scientific community over the years (programs Spectro[44–46] and Multimode[64–66]). In this Perspective, we will focus on VPT2-based models. Despite the known limitations of low-order pertubative methods in the treatment of large amplitude motions and the challenging task for anharmonic methods to treat correctly explicit solvent-solute interactions, it has been shown that VPT2 is reliable in the treatment of low-lying vibrational states (i.e. fundamentals and first overtones and combination bands) of semi-rigid, isolated systems, on which this perspective is focused. Indeed, the VPT2 approach is particularly appealing in connection with the computation of third and a subset of fourth energy derivatives by means of numerical differentiation of analytical second derivatives computed by methods rooted in the density functional theory (DFT) and, especially, by hybrid[48,73–83] or double-hybrid[84–86] functionals. The reliability of the results can be further improved by adding DFT anharmonic corrections to the harmonic contributions obtained with more reliable methods (in particular CCSD(T) with at least cc-pVTZ basis sets)[73,82,83,87–93]. Although basic VPT2 is plagued by resonances, robust and general procedures have been proposed over the years to overcome this problem[44,49,52,83,94–96]. Conversely, much less work has been performed

concerning IR intensities or Raman activities.[5] In the framework of perturbative treatments, after the pioneering work of Handy and co-workers[46], general implementations of IR intensities have been reported by several groups[45,58,96–99]. Recently, we have introduced a general treatment of transition properties, which straightforwardly includes, together with IR intensities, also Raman and vibrational circular dichroism (VCD) spectroscopies[100]. This approach has been also extended to take into account non-equilibrium solvent effects on vibrational (e.g. IR or VCD) transition intensities[101–103]. On these grounds, we report in the following a more detailed analysis of IR and Raman spectra of medium-size molecules and complexes including the effects of both mechanical and electrical anharmonicity, with focus on isolated systems in the gas phase or low-temperature rare-gas matrix environments. Extension to condensed phases can be then envisaged either by means of discrete/continuum solvent models[102,104,105] and/or combining time-independent gas phase results with time-dependent evaluations of solvent shifts[106].

In order to provide and validate a computational strategy applicable also to quite large systems, for which the affordable levels of electronic structure calculations are limited, we have resorted to the B3LYP functional coupled to basis sets of different sizes, up to aug-cc-pVQZ. From these tests, we can confirm that aug-cc-pVTZ provides for DFT computations nearly converged wavenumbers and intensities. Additionally, we investigate if smaller and more effective basis sets (in particular the SNSD and SNST families[107–111] recently proposed by our group) could be sufficiently accurate for effective studies of IR and Raman intensities. Reduced dimensionality approaches are further shortly discussed as additional tools for increasing the size of investigable systems. Finally, a discussion will be dedicated to the possibility of further improving the overall accuracy by mean of hybrid computational approaches[73,82,83,87–93]. Concerning Raman spectra, in the present work we will confine ourselves to static (low-energy) computations, postponing the inclusion of frequency-dependence to forthcoming studies.

The paper is organized as follows: after providing a short summary of VPT2 computations for wavenumbers and intensities (section 2), we define an effective computational strategy applicable to larger systems and analyze the functionals and basis set effects for a set of small-to-medium size closed- and open-shell benchmark systems (section 3). Next, IR and Raman spectra of some semi-rigid and flexible medium-size molecular systems are simulated and analyzed in sections 4 and 5, highlighting the fact that the anharmonic spectra provide more accurate (band positions) and more detailed (number of transitions) information than simple harmonic computations, thus enabling the correct interpretation of the experimental findings. The possible pathways toward feasible computations for larger molecular systems are presented in section 6, while the strategies to improve accuracy, for both band position and transition intensities are discussed in section 7. General conclusions and perspectives are given in the last section.

2 Theoretical background

As mentioned in the introduction, second-order vibrational perturbation theory (VPT2) is particularly appealing to treat medium-to-large systems. Among the available VPT2 models[39,42–44,46,49,50,98,112–114], we have developed a general framework to compute

thermodynamic properties, vibrational energies and transition intensities from the vibrational ground state to fundamentals, overtones and combination bands.[49,50,98,100,115] One strength of the VPT2 approach comes from its cost efficiency to compute accurate vibrational properties, at least for medium-size semi-rigid systems, in particular when applied to a fourth-order normal mode representation of the anharmonic force field. Moreover, difficulties related to the electronic structure computations necessary to explore the multidimensional anharmonic potential energy surface can be overcome with purposely tailored reduced-dimensionality VPT2 models[11]. The combinations of the anharmonic thermodynamic properties, vibrational energies and intensities allow to simulate very accurate vibrational spectra of single molecules or mixtures of several species or conformers, which can be directly compared with experimental data. For simplicity, the theoretical background presented in the following is intended for Abelian symmetry groups, that is with no degeneracy present. Finally, for reasons of compatibility with previous works, we have preferred to adopt units commonly used in the spectroscopic literature (instead of SI units), namely cm^{-1} for vibrational wavenumbers, km mol^{-1} for infrared intensities, and $\AA^4$ u^{-1} for Raman activities (1 $\AA$ = 1.0×10^{-10} m).

2.1 Vibrational energies

For a system with N internal degrees of freedom, the vibrational energies of the states of interest are given by[39,44,49],

$$\text{Fundamentals:}\nu_{1_i}=\omega_i+2\chi_{ii}+\frac{1}{2}\sum_{\substack{j=1\\j\neq i}}^{N}\chi_{ij} \quad (1)$$

$$\text{Overtones:}\nu_{2_i}=2\omega_i+6\chi_{ii}+\sum_{\substack{j=1\\j\neq i}}^{N}\chi_{ij} \quad (2)$$

$$\begin{aligned}\text{Combinations:}\nu_{1_i1_j} &= \omega_i+\omega_j+2\chi_{ii}+2\chi_{jj}+2\chi_{ij}\\ &\quad+\tfrac{1}{2}\sum_{\substack{k=1\\k\neq i,j}}^{N}\left[\chi_{ik}+\chi_{jk}\right]\\ &= \nu_{1_i}+\nu_{1_j}+\chi_{ij}\end{aligned} \quad (3)$$

where the anharmonic χ matrix has the form[39,44,49,50,115],

$$16\chi_{ii}=k_{iiii}-\frac{5{k_{iii}}^2}{3\omega_i}-\sum_{\substack{j=1\\j\neq i}}^{N}\frac{\left(8{\omega_i}^2-3{\omega_j}^2\right){k_{iij}}^2}{\omega_j\left(4{\omega_i}^2-{\omega_j}^2\right)} \quad (4)$$

Europe PMC Funders Author Manuscripts

$$
\begin{aligned}
4\chi_{ij} = \; & k_{iijj} - \frac{2\omega_i {k_{iij}}^2}{4{\omega_i}^2 - {\omega_j}^2} - \frac{2\omega_j {k_{ijj}}^2}{4{\omega_j}^2 - {\omega_i}^2} \\
& - \frac{k_{iii}k_{ijj}}{\omega_i} - \frac{k_{jjj}k_{iij}}{\omega_j} \\
& + \sum_{\substack{k=1 \\ k\neq i,j}}^{N} \left[\frac{2\omega_k \left({\omega_i}^2 + {\omega_j}^2 - {\omega_k}^2\right) {k_{ijk}}^2}{\Delta_{ijk}} - \frac{k_{iik}k_{jjk}}{\omega_k} \right] \\
& + \frac{4\left({\omega_i}^2 + {\omega_j}^2\right)}{\omega_i \omega_j} \sum_{\tau=x,y,z} B_e^{\tau} \left(\zeta_{ij}^{\tau}\right)^2 \\
\Delta_{ijk} = \; & {\omega_i}^4 + {\omega_j}^4 + {\omega_k}^4 - 2\left({\omega_i}^2{\omega_j}^2 + {\omega_i}^2{\omega_k}^2 + {\omega_j}^2{\omega_k}^2\right)
\end{aligned}
\tag{5}
$$

ω_i is the harmonic wavenumber (in cm^{-1}) associated to mode i, B_e^{τ} is the diagonal inertial tensor of the molecule at equilibrium geometry and ζ_{ij}^{τ} the Coriolis constant coupling mode i and j along the rotation axis I_{τ}. Finally, k_{ijk} and k_{ijkl} are the third and fourth derivatives of the potential energy V with respect to the dimensionless normal coordinates $\boldsymbol{q}$, also referred to as cubic and quartic force constants,

$$
k_{ijk} = \frac{\partial^3 V}{\partial q_i \partial q_j \partial q_k} \quad \text{and} \quad k_{ijkl} = \frac{\partial^4 V}{\partial q_i \partial q_j \partial q_k \partial q_l}
$$

It should be noted that a less general-purpose notation with respect to Refs.[49,50,115] has been adopted here since we consider only energy minima.

At this point, a discussion about the problem of resonances in the VPT2 treatment is appropriate. More precisely, the matter at hand is when resonances result in vanishing or nearly-vanishing denominators in the formulae used to compute the quantities of interest. Vibrational energies, for instance, suffer from the presence of so-called Fermi resonances, that is when the wavenumber of a mode is twice the wavenumbers of one mode ($\omega_i \approx 2\omega_j$, type I) or equal to the sum of the wavenumbers of two modes ($\omega_i \approx \omega_j + \omega_k$, type II), which result in an improper account of the anharmonic correction. Workarounds have been proposed in the literature to overcome such a problematic situation[44,52,95,96]. A commonly adopted scheme is based on a two-step procedure[44,49]. First, resonant terms are identified by mean of an *ad hoc* test, such as the one proposed by Martin *et al.*[52] and successively removed, which correspond to the deperturbed VPT2 (DVPT2). In the second step, the discarded terms are reintroduced through a variational treatment. We refer to the whole procedure as the generalized VPT2 (GVPT2), and this approach has been recognized to give very accurate results[45,76–79,82,85,92,93]. The Martin test[52] used in our GVPT2 implementation relies on a double control on the difference in wavenumber ($|\omega_i - (\omega_j + \omega_k)| \leq \Delta_{\omega}$ where $j = k$ for type I) and on the magnitude of the possibly resonant terms[49],

$$
\begin{aligned}
\text{For type I}, \Delta_{ij}^1 &= \frac{{k_{ijj}}^4}{256(2\omega_j - \omega_i)^3} \geq \mathscr{K}^I \\
\text{For type II}, \Delta_{ijk}^1 &= \frac{{k_{ijk}}^4}{64(\omega_j + \omega_k - \omega_i)^3} \geq \mathscr{K}^{II}
\end{aligned}
$$

where $\mathscr{K}^I$ and $\mathscr{K}^{II}$ are empirically defined thresholds. Default, reliable values are provided internally for these parameters but can be easily modified by the user. Moreover, it is

possible to redefine the resonant terms, which can be convenient to allow a direct comparison with the results from other theoretical approaches, as well as to test the influence of any specific interaction on the overall results.[92] Terms defined as resonant are removed and subsequently treated variationally.

From a practical point of view, the quality of vibrational wavenumbers computed at the GVPT2 level[39,44], as implemented in the GAUSSIAN package[49,50,83] has been already well documented[74,81,82,85,92,93,116,117]. Here we will only discuss the computational requirements for the force field evaluation. First, equilibrium structures have to be optimized using tight convergence criteria (maximum forces and displacements lower than 1.5×10^{-5} Hartree/Bohr and 6×10–5 Å, respectively). The semi-diagonal quartic force field is obtained by numerical differentiation of the analytical second derivatives along each normal coordinate (with the standard 0.01 Å step). In order to get accurate results, all computations are done with at least an ultrafine integration grid (99 radial shells and 590 angular points per shell) for the numerical integrations to obtain the two-electron integrals and their derivatives. Concerning the nearly-resonant contributions, the test proposed by Martin *et al.*[52] is applied with the following settings $\Delta_\omega = 200$ cm^{-1}, $\mathscr{K}^I = 1$ cm^{-1}, $\mathscr{K}^{II} = 1$ cm^{-1} used by default.

However, as explained in ref.[115], this two-step procedure suffers from a direct dependency on the empirical parameters (namely $\Delta\omega$, $\mathscr{K}^I$, $\mathscr{K}^{II}$), which can lead to unexpected behaviours about the thresholds used when analyzing an ensemble of force fields for a given structure or when studying a series of structures along a reaction path. An alternative approach proposed by Kuhler, Truhlar and Isaacson, called degeneracy-corrected PT2 (DCPT2), does not use any parameter since all potentially resonant terms are rewritten in a non-resonant way[95]. While this method offers a consistent solution to the problem of resonances, the transformation can be ill-suited far from resonances. To cope with this shortcoming, we have introduced the hybrid DCPT2-VPT2 (HDCPT2)[115] scheme, which mixes the DCPT2 and standard VPT2 approaches by mean of a transition function without the need for an actual evaluation and identification of the resonant terms. This makes this method particularly suited for black-box procedures and to control the reliability of the thresholds used for the Martin test.

2.1.1 Reduced dimensionality vibrational perturbative approach—In reduced-dimensionality VPT2 computations, a set of M normal modes for which anharmonic wavenumbers will be evaluated, that we will refer to as the active modes, is defined. The choice of active modes is related to the system under study, for instance the most intense transitions in the IR or Raman spectrum, a range of energy or a molecular fragment, such as a molecular probe. In practice, numerical differentiation is performed along the normal coordinates of active modes, so that for any non-linear N-atomic system, $2M + 1$ Hessians need to be computed, instead of $6N - 11$. These lead to a reduced number of force constants available for the perturbative treatment, that is, assuming that index i corresponds to an active mode and j and k are inactive modes, all the cubic force constants where index i is present at least once (i.e. k_{ijk}, k_{ijj}, k_{iik}, k_{iii}) and all k_{iijj} and k_{iiij} quartic force constants. However, a limited number of cubic force constants (terms including only j and k indices)

will not be evaluated. In practice, this omission will have an impact with respect to the full-dimensionality treatment only when a subset of the strongly coupled vibrations is included in the set of active modes. Indeed, there are only two terms in Eq. 5 which might not be computed, namely:

$$\Delta_j = \frac{k_{jjj} k_{iij}}{4\omega_j} \quad \text{and} \quad \Delta_{jk} = \frac{k_{iik} k_{jjk}}{4\omega_k} \qquad (6)$$

The first term, Δ_j, should not be omitted if both k_{jjj} and k_{iij} are large. Since $k_{iij}/4\omega_j$ is known, it is possible to have a qualitative estimate of the impact of the whole term in the calculation of χ_{ij}. If it is very small, then it is likely that Δ_j will give a small contribution and can be safely neglected. A larger value of k_{iij} reflects a significant coupling between modes *i* and *j*, meaning that mode *j* must be also included in the set of active modes. Chemical intuition can also help to assess more precisely the magnitude of $k_{jjj}k_{iij}$ by noting that k_{jjj} will be important only if mode *j* is strongly anharmonic. In such a case, mode *j* must be included in the set of active modes to be treated anharmonically. If the numerical differentiation along *j* is too cumbersome and does not have an interest *per se* (e.g. it is not in the wavenumber range under study), an alternative approach would be to include only the missing term k_{jjj} through numerical evaluation of one-dimensional energy third derivatives, a task much less computationally demanding than the complete computation. The second term, Δ_{jk}, reflects the coupling of mode *k* with both modes *i* and *j*. As before, the known k_{iik} can be used to guess the possible influence of the whole term, which will not contribute to Eq. 5 if $k_{iik}/4\omega_k$ is negligible, i.e. if *i* and *k* are uncoupled. On the other hand, for large k_{iik} constants, the whole Δ_{jk} term is not negligible if mode *j* is also strongly coupled to mode *k*. A more detailed analysis has been given in Ref.[11]. Here we just summarize that the reduced-dimensionality approach can be safely applied if all modes which are strongly coupled are included simultaneously in the VPT2 computations, so that the necessary force constants are evaluated. The choice of normal modes can be based on “chemical intuition” (the geometrical confinement of vibrations and the spanned wavenumber range, since the vibrations localized in different regions of the molecular systems and with significantly different wavenumbers are unlikely to be strongly coupled) and followed by appropriate validation[11], or derived from lower-level electronic structure computations, resonance conditions, or normal mode similarity (See Ref.[118] and references therein). Finally, it should be noted that if *j* is also in the active set, both terms are taken into account, while only the second one will be available if mode *k* is active instead.

2.2 Band intensities

The derivation of equations for the transition moments at the anharmonic level is made difficult by the need to account for both the anharmonicity of the potential energy surface (PES) and of the property of interest. Due to the complexity of such a treatment, various approximations have been employed, in particular by considering independently the wave function and the property, so that different levels of theory can be applied to each term and only one of them is treated beyond the harmonic approximation[119,120]. Following the first complete derivation by Handy and co-workers[121], we adopted the alternative approach presented by Vázquez and Stanton[58] and proposed a general formulation for any property

function of the normal coordinates or their associated momenta, which can be expanded in the form of a polynomial truncated at the third order. In this work, we will only consider the molar absorption coefficient $\varepsilon\left(\bar{\nu}_0\right)$ and Raman scattering at 90° for any polarization of an incident light with perpendicular polarization $\partial\sigma\left(\bar{\nu}_0\right)/\partial\Omega_{100}$,

$$\varepsilon\left(\bar{\nu}_0\right)=\frac{8\pi^3\mathcal{N}_A\bar{\nu}_0}{3000\ln(10)\,hc\,(4\pi\varepsilon_0)}\sum_o\sum_e D_{o,e}\delta\left(\varepsilon_e-\varepsilon_o-\bar{\nu}_0\right) \quad (7)$$

$$\frac{\partial\sigma\left(\bar{\nu}_0\right)}{\partial\Omega}=\frac{h}{8\pi^2c}\sum_o\sum_e\frac{\left(\bar{\nu}_0-(\varepsilon_e-\varepsilon_o)\right)^4 S_{o,e}}{45\,(\varepsilon_e-\varepsilon_o)\left(1-\exp\left(-\frac{hc(\varepsilon_e-\varepsilon_o)}{k_BT}\right)\right)} \quad (8)$$
$$\times\,\delta\left(\varepsilon_e-\varepsilon_o-\bar{\nu}_0\right)$$

where $\bar{\nu}_0$ is the wavenumber of the incident light and δ is the Dirac function. The summation runs over all initial states o and final states e with wavenumbers ε_o and ε_e, respectively.

The static dipole strength $D_{o,e}$ and the Raman activity $S_{o,e}$ are given by,

$$D_{o,e}=\left|\langle\boldsymbol{\mu}\rangle_{o,e}\right|^2 \quad (9)$$

$$S_{o,e}=45{\alpha_{o,e}}^2+7{\beta_{o,e}}^2 \quad (10)$$

with $\boldsymbol{\mu}$ the electric dipole, $a_{o,e}$ the mean polarizability and ${\beta_{o,e}}^2$ the anisotropy term,

$$\begin{aligned}\alpha_{o,e}=&\ \tfrac{1}{3}\left[\langle\alpha_{xx}\rangle_{o,e}+\langle\alpha_{yy}\rangle_{o,e}+\langle\alpha_{zz}\rangle_{o,e}\right]\\ {\beta_{o,e}}^2=&\ \tfrac{1}{2}\left[\langle\alpha_{xx}\rangle_{o,e}-\langle\alpha_{yy}\rangle_{o,e}\right]^2+\tfrac{1}{2}\left[\langle\alpha_{yy}\rangle_{o,e}-\langle\alpha_{zz}\rangle_{o,e}\right]^2\\ &+\tfrac{1}{2}\left[\langle\alpha_{zz}\rangle_{o,e}-\langle\alpha_{xx}\rangle_{o,e}\right]^2\\ &+3\left[{\langle\alpha_{xy}\rangle_{o,e}}^2+{\langle\alpha_{yz}\rangle_{o,e}}^2+{\langle\alpha_{zx}\rangle_{o,e}}^2\right]\end{aligned}$$

The general formulation to compute the transition moments of the electric dipole vector $\langle\boldsymbol{\mu}\rangle_{o,e}$ and polarizability tensor $\langle\boldsymbol{\alpha}\rangle_{o,e}$ has been given in Ref.[100]. Since the properties of interest here depend on the normal coordinates and not on their conjugate momenta, we can use a more compact formula for fundamentals than the one used in Ref.[100],

$$
\begin{aligned}
\langle P^a\rangle 0,1_i=&\frac{P^a_i}{\sqrt{2}}+\frac{1}{4\sqrt{2}}\sum_j P^a_{jji}\\
&-\frac{1}{8\sqrt{2}}\sum_{jk}k_{ijkk}P^a_j\left[\frac{1}{\omega_i+\omega_j}-\frac{1-\delta_{ij}}{\omega_i-\omega_j}\right]\\
&-\frac{1}{8\sqrt{2}}\sum_{jk}\left\{k_{ijk}P^a_{jk}\left(\frac{1}{\omega_i+\omega_j+\omega_k}-\frac{1}{\omega_i-\omega_j-\omega_k}\right)\right.\\
&\left.+\frac{2k_{jkk}}{\omega_j}P^a_{ji}\right\}\\
&+\frac{1}{2\sqrt{2}}\sum_{jk}\left(\sum_\tau B^\tau_e\zeta^\tau_{ik}\zeta^\tau_{jk}\right)P^a_j\left\{\frac{\sqrt{\omega_i\omega_j}}{\omega_k}\left(\frac{1}{\omega_i+\omega_j}+\frac{1-\delta_{ij}}{\omega_i-\omega_j}\right)\right.\\
&\left.-\frac{\omega_k}{\sqrt{\omega_i\omega_j}}\left(\frac{1}{\omega_i+\omega_j}-\frac{1-\delta_{ij}}{\omega_i-\omega_j}\right)\right\}\\
&+\frac{1}{16\sqrt{2}}\sum_{jkl}k_{ikl}k_{jkl}P^a_j\left\{\frac{4\omega_j\left(\omega_k+\omega_l\right)\left(1-\delta_{ij}\right)\left(1-\delta_{ik}\right)\left(1-\delta_{il}\right)}{\left({\omega_j}^2-{\omega_i}^2\right)\left[\left(\omega_k+\omega_l\right)^2-{\omega_i}^2\right]}\right.\\
&+\frac{\left(\omega_k+\omega_l\right)\left[\left(\omega_k+\omega_l\right)^2-3{\omega_i}^2\right]\delta_{ij}\left(1+\delta_{ik}\right)\left(1-\delta_{il}\right)}{\omega_i\left[\left(\omega_k+\omega_l\right)^2-{\omega_i}^2\right]^2}\\
&\left.+\frac{4\omega_j\left(3\omega_k+4\omega_i\right)\left(1-\delta_{ij}\right)\left(1-\delta_{ik}\right)\delta_{il}}{\omega_k\left({\omega_j}^2-{\omega_i}^2\right)\left(\omega_k+2\omega_i\right)}\right\}\\
&+k_{ijk}k_{llk}P^a_j\left\{\frac{\delta_{ij}}{\omega_i\omega_k}\left(1+\frac{2\delta_{ik}\delta_{il}}{9}\right)\right.\\
&+\frac{4\omega_j\left(1-\delta_{ij}\right)\left(1-\delta_{ik}\right)\left(1-\delta_{il}\right)}{\omega_k\left({\omega_j}^2-{\omega_i}^2\right)}\\
&\left.+\frac{4\omega_j\delta_{ik}\left(1-\delta_{ij}\right)}{\omega_i\left({\omega_j}^2-{\omega_i}^2\right)}\left(1+\frac{2\delta_{ij}}{3}\right)\right\}
\end{aligned}
\tag{11}
$$

where P^a is a cartesian component of the electric dipole or an element of the polarizability tensor and δ_{ij} is the Kronecker delta. $\boldsymbol{P}_i$, $\boldsymbol{P}_{ij}$ and $\boldsymbol{P}_{ijk}$ are respectively the first, second and third derivatives with respect to the dimensionless normal coordinates,

$$
\boldsymbol{P}_i=\frac{\partial\boldsymbol{P}}{\partial q_i};\boldsymbol{P}_{ij}=\frac{\partial^2\boldsymbol{P}}{\partial q_i\partial q_j};\boldsymbol{P}_{ijk}=\frac{\partial^3\boldsymbol{P}}{\partial q_i\partial q_j\partial q_k}
$$

For overtones and combination bands, simpler formulae are obtained, respectively,

$$
\begin{aligned}
\langle P^a\rangle_{0,2_i}=&\frac{1}{2\sqrt{2}}P^a_{ij}\\
&+\frac{1}{4\sqrt{2}}\sum_k k_{ijk}P^a_k\left(\frac{1}{\omega_i+\omega_j-\omega_k}-\frac{1}{\omega_i+\omega_j+\omega_k}\right)
\end{aligned}
\tag{12}
$$

$$\langle P^a \rangle_{0,1_i 1_j} = \frac{1}{2} P^a_{ij} + \frac{1}{4} \sum_k k_{ijk} P^a_k \left(\frac{1}{\omega_i + \omega_j - \omega_k} - \frac{1}{\omega_i + \omega_j + \omega_k} \right) \quad (13)$$

Similarly to vibrational energies, Eqs. 11, 12 and 13 are plagued by the existence of potential singularities, which lead to excessive contributions from the anharmonic terms. In addition to the Fermi resonances described above, 1-1 resonances ($\omega_i \approx \omega_j$) are present for fundamental transitions. The protocol used to avoid unphysical contributions in the anharmonic correction is similar to the one used for energies. Terms identified as resonant through *ad hoc* tests are removed from the calculations. Contrary to the GVPT2 model used for wavenumbers, this step is not followed by any variational treatment of the resonant terms. In practice, the same Martin test is adopted to find Fermi resonances. For 1-1 resonances, the test described in Ref.[100] is used here. It relies on two complementary conditions. The first one is the difference in wavenumbers,

$$|\omega_i - \omega_j| \leq \Delta_\omega^{1-1}$$

The second one is based the magnitude of the numerator and uses two thresholds depending on the term, $\mathscr{K}_1^{1-1}$ for cubic terms and $\mathscr{K}_2^{1-1}$ for quartic and Coriolis terms,

$$|k_{ijk} k_{lmn}| \geq \mathscr{K}_1^{1-1}$$
$$|k_{ijkl}| \geq \mathscr{K}_2^{1-1}; \left| \sum_\tau B_e^\tau \zeta_{ik}^\tau \zeta_{jk}^\tau \right| \geq \mathscr{K}_2^{1-1}$$

with the default values as following: $\Delta_\omega^{1-1} = 2\,\mathrm{cm}^{-1}$, $\mathscr{K}_1^{1-1} = 1\,\mathrm{cm}^{-2}$, $\mathscr{K}_2^{1-1} = 1\,\mathrm{cm}^{-1}$.

2.3 Thermodynamics

The relative abundance of each species (e.g. conformer) in a mixture under a given set of conditions, such as the temperature, can be estimated from their respective vibrational partition function Q_{vib}. The simple perturbation theory (SPT) proposed by Truhlar and Isaacson offers a simple way to evaluate Q_{vib} at the anharmonic level[122]. In practice, the same formula as for the harmonic approximation is used,

$$\mathrm{Q_{vib}} = \frac{e^{\frac{-E_0}{k_B T}}}{\prod_{i=1}^{N}} \left(1 - e^{\frac{-hc\nu_{1_i}}{k_B T}} \right) \quad (14)$$

in which E_0 is the zero-point vibrational energy (ZPVE) and ν_{1i} is the fundamental energy associated to mode i, both computed at the VPT2 level.

The resonance-free formulation proposed by Schuurman *et al.*[123] was used for E_0 ,

Europe PMC Funders Author Manuscripts

$$E_0 = E_0^{(0)} + \sum_{i=1}^{N}\sum_{j=1}^{N}\left\{\frac{k_{iijj}}{32} - \sum_{k=1}^{N}\left[\frac{k_{iik}k_{jjk}}{32\omega_k} + \frac{{k_{ijk}}^2}{48\,(\omega_i+\omega_j+\omega_k)}\right]\right\} + Z_{\text{kinetic}} \quad (15)$$

where $E_0^{(0)}$ is the harmonic ZPVE, and

$$Z_{\text{kinetic}} = 16 \sum_{\tau=x,y,z} \mu_{\tau\tau}^{\text{eq}} \left[\sum_{i=1}^{N-1}\sum_{j=i+1}^{N}\left(\zeta_{ij}^{\tau}\right)^2\right]$$

$\mu_{\tau\tau}^{eq}$ is an element of the inverse inertia tensor at the reference geometry.

A more general definition of the ZPVE at the VPT2 level was proposed in Ref.[115], which could also be used for transition states.

To compute the fundamental energies ν_{1i}, the versatile HDCPT2 model was used to provide a resonance-free expression for the partition function. A complete derivation of eqs. 4 and 5 at the HDCPT2 level can be found in Ref.[115].

A final comment regards the proper treatment of torsional anharmonicity, which still represents a challenging aspect for accurate thermochemical calculations of complex molecules.[124–132] Here, we use a generalization to anharmonic force fields of the Hindered-Rotor Harmonic Oscillator (HRHO) model[124] that automatically identifies internal rotation modes and rotating groups during the normal-mode vibrational analysis. This approach employs an effective analytical approximation of the partition function for a one-dimensional hindered internal rotation that reproduces the accurate values with a maximum error of about 2% for a number of reference systems[124]. The one-dimensional rotor treatment is generalized to give useful approximations of multidimensional rotor thermodynamic functions, and in the Hindered-Rotor Anharmonic-Oscilattor (HRAO) model, is further coupled to the simple perturbation theory (SPT) approach to the partition function for the other internal degrees of freedom[115].

All computational models described in this section have been implemented by some of us, and are available within the GAUSSIAN suite of programs for quantum chemistry[133]. All VPT2 computations applied to generate IR and Raman spectra have been performed within GVPT2/DVPT2 approach, while the degeneracy-free HDCPT2 model has been used in order to evaluate thermodynamic properties.

3 Cost-effective computations of IR and Raman spectra: DFT functionals and basis sets

Models rooted into the density functional theory can be successfully applied to fairly large molecular systems, well beyond the capabilities of more sophisticated *ab initio* methods. DFT has proven to be very successful for the prediction of ground- and excited-state

equilibrium structures, as well as for the purpose of computational spectroscopy studies including a broad range of linear and nonlinear spectral responses, and of magnetic (NMR and EPR) parameters (see the recent review provided in Ref.[6] and references therein). However, the quality of the results depends strongly on a careful choice of the functional and of sufficiently flexible basis sets. In the field of vibrational spectroscopies the requirements are an accurate prediction of vibrational wavenumbers and reliable transition intensities, which in turn are related to the quality of potential energy and electric and/or magnetic properties surfaces, respectively. Let us first discuss the choice of functionals allowing the computation of vibrational wavenumbers with the accuracy required for quantitative comparisons with experiment. We will focus on hybrid[134–142] functionals, including also long-range[135,137,142] and dispersion-corrected[143,144], as well as meta-hybrid[138,139] models, in the prediction of anharmonic wavenumbers for a set of small-to-medium sized molecular systems, while the performance of significantly more computationally demanding double-hybrid approaches[145,146] will be postponed to section 7. All computations have been performed in conjunction with polarised basis sets of double-ζ quality supplemented by diffuse functions, mainly from the N07D/SNSD family[107–109,111]. From Figure 1 it is clear that standard hybrid functionals, in particular B3LYP and B97-1 provide very satisfactory results, while some of the most successful last-generation functionals (M06-2X[139] and ωB97X[142]) do not show a sufficient accuracy for spectroscopic studies. Based on this analysis, we will use the B3LYP functional in all our computations at the DFT level, while possible accuracy improvements by mean of hybrid schemes with the harmonic part computed at a higher level of theory will be discussed in section 7. The latter are usually more important for the high-wavenumber region (X-H stretching vibrations), which in most cases show larger errors than low-lying fundamentals (C-C, C=O stretches), as shown with the glycine conformers.[93,147] We also note that if the system under study can only be correctly treated by including dispersion interactions, a viable way to accurate spectroscopic studies is provided by Grimme's semi-empirical dispersion correction[143,148] added to the B3LYP functional[117,149].

The accuracy of anharmonic wavenumbers computed with the B3LYP[150] functional in conjunction with the polarized double-ζ basis set N07D[107–109,111] has been further demonstrated for several medium-to-large closed- and open-shell systems[11,81,82,85,99,151]. The N07D basis set has been constructed aiming at cost-effective computations of spectroscopic properties for medium-to-large molecular systems. N07D has been recently extended by consistently including diffuse *s* functions on all atoms, and one set of diffuse polarized functions (*d* on heavy atoms and *p* on hydrogens), leading to the new SNSD basis set which confirmed its effectiveness for computational spectroscopy studies of relatively large molecular systems, and different properties/spectroscopies[81,82,85,107–110,152] including the early results on IR and Raman spectra[93,153]. In this work we also consider an effective triple-ζ basis set, SNST (previously denoted as aug-N07T[152]) constructed by consistent inclusion of diffuse *s* functions starting from the N07T basis set. These basis sets allow the reliable prediction of excited-state properties[81,152], including rotatory strengths and transition dipole moments[152], and due to their construction are also expected to be well suited for IR intensities and Raman activities computations.

In this work, we provide further data on the applicability of the B3LYP/SNS(D/T) approach for the computations of Infrared (IR) intensities and Raman activities (RA), whose dependence on the electric dipole moment and polarizability derivatives lead to a stronger sensitivity to electron correlation and basis set extension effects[154–159]. Concerning the effect of correlation, it has been shown that converged IR intensities can be obtained at the CCSD(T) level in conjunction with basis sets of at least aug-cc-pVTZ quality[156,157,160]. In the DFT frameworks, hybrid functionals (e.g B3LYP) lead to the best agreement with the most refined post-Hartree-Fock methods[154]. Moreover, concerning composite schemes recently introduced to evaluate best estimates for IR intensities within the double-harmonic approximation[93,161], slow convergence to the CBS limit has been observed at the MP2 level, together with large effects of diffuse functions and rather small core-correlation corrections (CV) (the largest contributions being of a few km mol^{-1}, at most). The differences between MP2/ccpVTZ and MP2/cc-pVQZ IR intensities are in most cases on the order of 1-2 km mol^{-1} but variations as large as 15-20 km mol^{-1} [93] have been also found, while the effects of diffuse functions are on average of about 5 km mol^{-1}, but, in specific cases, reach 25-35 km mol^{-1}. On the other hand, the harmonic and anharmonic IR intensities computed at the B3LYP/SNSD level show remarkable agreement with converged CCSD(T) results and experimental data[160,162].

Similarly, the very few studies available on Raman activities have shown that the effects due to the electron correlation are less pronounced in comparison to those originating from the truncation of the basis set[159], and again DFT approaches are more efficient than their MP2 counterparts[155]. Thus, in the present work we will focus on the basis set convergence, following the findings reported by Schlegel *et al.*[154] for IR intensities and the fact that while Raman activities require larger basis sets than IR intensities, a purposely tailored mediumsized basis sets, able to describe correctly the tail region of the electron density can be developed (see for example the pVTZ basis set developed by Sadlej[163] or aug(sp)-cc-pVDZ recently proposed by Cheeseman and Frisch[159]). It should be noted that the absolute values of both IR intensities and Raman activities are rather difficult to determine experimentally, with inaccuracies of about 10%[157,158], so usually only the relative data are reported and used in spectroscopic analysis. For this reason we resort to the comparison with other theoretical values, obtained at the B3LYP level with aug-cc-pVXZ (AVXZ) basis sets[164,165] of double- to quadruple-ζ (X=D,T,Q) quality.

Taking into account benchmark studies available in literature, for both IR intensities[154,156,157,166,167] and Raman activities[155,166–171], we set up two benchmark sets considering small closed- and open-shell molecules with a variety of single and multiple bonds (benchmark set VIB67) and a few selected medium-sized molecular systems which can be considered as representatives of important biomolecule building blocks (benchmark set VIBbio100), in both cases considering only molecular systems which contain atoms from the first two rows of periodic table. Thus, the VIB67 benchmark set is composed of 15 molecules, in total 67 fundamental vibrations (CH^+, HF, NH, OH, CN, CO, NO, H_2O, H_2CO, H_2CN, C_2H_4, CH_2F_2, CH_3NH_2, CH_3OH, $HCONH_2$ and HCOOH); while the VIBbio100 benchmark set is composed of: furan, pyrrole, pyrimidine, glycine and phenyl radical, with over 100 fundamental vibrations. Results computed with the double- and triple-

ζSNS basis sets, SNSD and SNST respectively, have been compared to the ones obtained with the Dunning basis sets aug-cc-pVXZ[164,165]. For smaller molecules (set VIB67), basis sets up to aug-cc-pVQZ have been considered (X=D,T,Q), while for medium-size systems (set VIBbio100) the most expensive computations are performed at the B3LYP/aug-cc-pVTZ level (X=D,T).

Harmonic and anharmonic vibrational wavenumbers (in cm^{-1}), infrared intensities (in km mol^{-1}) and Raman activities (in $Å^4$ u^{-1}) computed for set of 7 bi-hetero-atomic closed- and open-shell molecules are listed in Table 1, while mean absolute errors (MAE) and maximum absolute errors |MAX| with respect to the B3LYP/aug-cc-pVQZ results computed over the whole VIB67 benchmark set are reported in Table 2. It can be noted that harmonic wavenumbers, IR intensities and Raman activities are essentially converged at the aug-ccpVTZ level, the average discrepancies with respect to aug-ccpVQZ results being lower than 3 cm^{-1}, 0.3 km mol^{-1} and 0.4 $Å^4$ u^{-1}, and maximum errors lower than 8 cm^{-1}, 1.0 km mol^{-1} and 1.0 $Å^4$ u^{-1}, respectively, but with basis set size reduced by about 50%. Among the least expensive basis sets, of double-ζ quality, which both include only about 25% of basis functions with respect to AVQZ, SNSD performs significantly better, in particular as far as anharmonic corrections are concerned; this finding is remarkable for hybrid QM/QM' schemes which have shown to be very effective for accurate studies of medium-to-large molecular systems[82,85,93,153,161]. Moreover, improved results for IR intensities and Raman activities can be obtained at an only slightly increased computational cost by using the purposely tailored triple-ζ basis set SNST, which contains on overall about 20% basis functions more that SNSD and aug-cc-pVDZ but about 40% less than those of the standard aug-cc-pVTZ. Performance of the aug-cc-pVDZ (AVDZ), SNST and SNSD basis sets are compared to aug-cc-pVTZ (AVTZ) also for the medium-sized molecules from the VIBbio100 benchmark set in Table 3. Also in this case the results with the SNSD basis set are better than those obtained with its double-ζ counterpart AVDZ, in particular for anharmonic contributions and harmonic wavenumbers, while an improved accuracy for IR intensities and Raman activities can be obtained with computations at the SNST level.

Considering the simulation of IR and Raman spectra, reliable relative intensities along with accurate band positions are sufficient to obtain a correct overall spectra line-shape/intensity pattern, which in turn is required for the analysis of experimental results. In this respect comparable results are obtained with all basis sets (AVTZ, AVDZ, SNST and SNSD) for the IR and Raman spectra of furan, presented in Figures 2 and 3, respectively. In fact, in all cases, a similar intensity pattern is obtained even in fully anharmonic spectral ranges, related to overtones and combination bands (3900-4800 cm^{-1}), the only significant discrepancy being related to the intensity of the 2_{17} overtone in the Raman spectra (at about 1670 cm^{-1}) overestimated by SNST computations, but correctly predicted by the SNSD basis set. Moreover, SNST and SNSD perform better than AVDZ as far as band positions are concerned, with the most visible difference for the intense IR transition at about 740 cm^{-1} or the Raman one at about 3160 cm^{-1}. On the whole, we can conclude that all considered basis sets provide reliable estimates of IR and Raman spectra. Therefore, the cost-effective SNSD basis set can be recommended for anharmonic computations. As it will be discussed in more details in section 7, we should mention that it is possible to improve the overall accuracy at a

reasonable computational cost by using hybrid models where the harmonic part is computed with larger basis sets, or at a higher level of theory.

4 Semi-rigid medium-size closed- and open-shell systems: Thymine and Phenyl radical

Combined IR and Raman spectroscopic studies, plotted and analyzed together, allow to obtain more detailed and precise information on the properties of molecules under study, in particular to identify and assign all fundamental transitions also for relatively large systems. Here we show that the analysis of experimental data can be complemented by the direct comparison of both kinds of spectra with their theoretical anharmonic counterparts, taking into account also intensities of overtones and combination bands. For Raman spectra it is a common procedure to correct the experimental scattering signal by applying a factor of $\nu^4/\Delta\nu_{vib}$[172] (with ν being the wavenumber of the scattered light and $\nu = \nu_{exc} - \Delta\nu_{vib}$, where ν_{exc} is the exciting light wavenumber) in order to obtain a signal that could be integrated over each band to obtain the relative integrated band areas, which are directly proportional to the calculated Raman scattering activities. This procedure allows to obtain data independent from specific experimental conditions, and also facilitate comparison between experimental and computed results. For such reason in most cases along this paper we will report Raman spectra line-shapes in terms of static Raman scattering activities in $Å^4\ u^{-1}$.

As an example of integrated IR and Raman studies of biomolecule building blocks isolated in low-temperature matrices, we will discuss the case of the nucleic-acid base thymine, comparing the simulated spectra to the experimental measurements performed by Szczepaniak *et al.*[173]. It is evident from Figure 4 that, although all high-wavenumber transitions are present in both IR and RA spectra, the intensity distribution is significantly different between both spectra. Simulated IR and Raman anharmonic spectra agree very well with their experimental counterparts, for both the band positions and the intensity pattern (intense RA transitions predicted by theory fall outside the region of sensitivity of the Raman instrument). It is also clear that several observed transitions are missing in the harmonic spectra, and these drawbacks can not be resolved by simply scaling the computed harmonic wavenumbers. At variance, computations beyond the double-harmonic approximation allow to assign also non-fundamental transitions, as shown in Figure 5 for the 2800-3800 cm^{-1} wavenumber range. For example, the band at 2899 cm^{-1} has been tentatively assigned to the overtone 2_{11}, while our results suggest an alternative assignment to the $1_{10}1_{11}$ combination transition. Moreover, several additional weak features can be assigned to overtones or combination bands, some of them easily observed in the IR spectrum (e.g. 2_8), others in the RA experiment (e.g. 2_{12}). All fundamental transitions and selected overtones and combination bands observed in the 2800-3800 cm^{-1} wavenumber range are also listed in Table 4, and compared to experimental results. Our computations agree with previously proposed assignments, suggesting that for the doublet at 2997 cm^{-1} and 2987 cm^{-1} assigned in Ref.[173] to the Fermi resonance between asymmetric in-plane CH-stretching vibration of CH_3 and some combination band, the higher-wavenumber transition is related to the 1_91_{16} combination and the lower one to the 1_4 fundamental band. Most of the anharmonic wavenumbers agree with experiment within 5 cm^{-1}, with the largest

discrepancies of about 25 cm^{-1} observed for the C-H stretching wavenumbers of CH_3 and an overall mean absolute error (MAE) of 10 cm^{-1}. It can be noted that improved accuracy can be expected from the correction of harmonic wavenumber by means of hybrid approaches discussed in Section 7.

Direct simulations of reliable IR and Raman spectra, already valuable for the analysis of experimental outcomes for closed-shell systems, are even more important for open-shell species, for example organic free radicals, playing a significant role in a number of processes of biological, technological or astrochemical relevance[174]. An increased difficulty to perform experimental spectroscopy studies of radicals is related to their short life-time and high reactivity, so that experimental outcomes might be cumbersome to interpret, even in terms of appropriate identification of molecular species[175,176]. In most cases the studies of radicals involve quite elaborate integrated experimental procedures combining several complementary spectroscopic techniques and possibly a few precursors, with accurate computational data playing an essential supporting role. In this context, analysis of experimental outcomes requires to dissect between the spectral features related to the species under study, precursors, other possible photoproducts, and any possible impurities. In principle, it might happen that some significant transitions are assigned to other species and ruled out. In fact, in several cases experimental spectra have been reassigned (e.g. for F_2NO[87]) or re-investigated (e.g. for vinyl radical[81,177–180]) based on theoretical suggestions. In this frame, computations of fully anharmonic IR and Raman spectra for several species possibly present in the experimental mixture and/or including a few sets of isotopically substituted precursors, can be recommended. As an example, we refer to a recent study of phenyl radical[153], which allowed us to critically analyze the IR[181] and Raman[182] spectra with an unprecedented accuracy, suggesting a re-investigation of the spectral zone where bands due to precursor and water impurities are clearly present. Such an analysis can be illustrated by the comparison of simulated Raman spectra of nitrosobenzene and phenyl radical, with the experimental Raman spectrum[182] of their mixture (obtained after prolonged excimer laser irradiation at 308 nm). Figure 6 shows, that several bands belonging to either phenyl radical or nitrosobenzene can be identified in the experimental spectrum, but at the same time several remaining peaks are due to side products, or impurities. Our computational model makes feasible the simulation of spectra taking into account quite large numbers of species possibly present in the experimental mixture. This, in our opinion, would facilitate analysis and assignment by direct comparison with detailed experimental data, increasing the accuracy and reliability of reported experimental results.

5 Flexible molecules: Butane and Glycine Conformers

Several important molecular systems show a few nearly isoenergetic isomers and/or conformers, which are often concomitantly present in experimental mixture. In such cases analysis of experimental outcomes is further complicated as in principle all relevant low-energy minima should be considered, taking also into account their relative abundances. The latter can be estimated theoretically, based on the computed free energies. Taking into account the recent progress in the development of composite schemes aiming at an accurate prediction of thermochemical properties[183–188], it has been recognized that for larger systems the factor limiting the accuracy of thermochemical protocols will increasingly be

related to the vibrational properties[189]. A protocol, recently proposed by the present authors[115], briefly described in Section 2, allows for a rather straightforward and fully resonance-free computation of thermodynamic properties beyond the rigid-rotor harmonic-oscillator (RRHO) model. It combines the evaluation of resonance-free ZPVE with HDCPT2 wavenumbers used to evaluate degeneracy-corrected partition functions within the SPT model and including also an automatic treatment of internal rotations through the hindered-rotor model. Then, the spectra of complex molecular mixtures can be simulated by computation of contributions of all single conformers/isomers, weighted by theoretical Boltzmann populations. Such simulations allow to match the experimental conditions, for example by taking into account temperature effects. In this work the aforementioned approach has been applied to simulate the IR and Raman spectra of butane and the Raman spectra of glycine, in the latter case complementing recent works on accurate computations of its structure, thermodynamic and spectroscopic parameters from CC and CC/DFT schemes[93,147,190].

For butane, two relatively stable configurations *anti*- and *gauche*- contribute to the overall spectra at room temperature. Their relative weights of 64% and 36% have been computed with the SPT hindered-rotor anharmonic-oscillator (HRAO) model with all vibrational computations performed at the B3LYP/SNSD level of theory and electronic energy difference adjusted based on the best theoretical estimates recently reported by Császár *et al.*[191]. Figure 7 compares the overall (SUM) spectra of butane in the C-H stretching region, and single contributions from *anti*- and *gauche*- to experimental gas phase IR[192] and Raman[193] spectra in the 3200–2700 cm^{-1} wavenumber range. First, it is evident that both conformers yield rather different spectral patterns, so both need to be considered in order to simulate overall spectral shape. In fact, although the main spectral features are related to the more abundant *anti*- conformer, the agreement with experiment increases when the contributions from the *gauche*- one are also added. The butane IR and Raman spectra have been recently simulated[194] by VSCF-based computations[195], but taking into account only the *anti*- conformer due to high computational cost of the underlying electronic structure computations defining the PES and PS, and harmonically-derived expressions for intensities in Raman spectra. At variance, the theoretical approach used in the present work, being based on relatively inexpensive computations (yet retaining comparable accuracy of QM level), does not require unnecessary restrictions for the number of conformers to be considered (at least for mediumsize molecules). Moreover, both IR and Raman anharmonic intensities have been computed considering all fundamental transitions, overtones (2_i) and combination bands (1_i1_j) starting from the ground vibrational state, leading to an accurate simulation in all spectral regions. For IR spectra a very detailed comparison with the gas phase experiment is possible, with the latter reported in the NIST database[192]. Figure 8 shows that the anharmonic computations lead to a better agreement for the band positions, but also introduce several new spectral features related to non-fundamental transitions. The latter effect is well illustrated by the inset related to the 2600–1600 cm^{-1} spectral range where harmonic contributions yield vanishing spectra while anharmonic computations very well reproduce positions and band patterns in this very low-intensity spectral zone.

Glycine is an example of a quite simple molecule with a rather complex PES characterized by several local minima separated by low-energy barriers and large conformational flexibility due to the presence of three internal rotational degrees of freedom. Among the six low-lying conformers, at least five (namely Ip/ttt, IIn/ccc, IIIp/tct, IVn/gtt and VIp/ttc, see Figure 9) have been observed experimentally in different spectroscopic measurements (Microwave, IR, Raman) and in conditions ranging from the gas phase[196–204] to low-temperature rare-gas matrices[205–208] or helium nanodroplets[209]. Our recent state-of-the-art quantum-chemical computations[93,147,190] allowed to complement available experimental data leading to a better understanding of the whole potential energy surface governed by soft degrees of freedom, as well as to complete structural, thermodynamic, and spectroscopic characterization of glycine conformers along with suggestion of new experiments that would allow the unequivocal detection of "elusive" conformers. In particular, it has been shown that, although the rigid-rotor harmonic-oscillator (RRHO) approximation provides semi-quantitative results for enthalpies and free energies at 15K, a more refined model is required to get qualitatively correct predictions of the relative population of conformers at higher temperatures (e.g. 410 K). This is due to the fact that the entropy of the IIIp/tct rotamer is strongly overestimated by the RRHO model, and only the full HRAO approach is able to provide a reasonable relative free energy of this conformer. Here we extend our study of glycine conformers to the Raman spectra, with the wavenumbers computed at the hybrid CC/DFT level described in detail in reference[93] and both harmonic and anharmonic Raman activities computed at the B3LYP/SNSD level. Figure 9 reports the spectra of all six low-lying conformers, the sum spectrum of the three most stable ones Ip/ttt, IIn/ccc and IIIp/tct, with each contribution weighted according to the relative Boltzmann population at 410 K considering also the IVn/gtt and Vn/gct conformational cooling (IVn/gtt→Ip/ttt and Vn/gct→IIIp/tct), and the spectrum with additional minor contributions (1%) from the IVn/gtt, Vn/gct and VIp/ttc conformers. The good accuracy of CC/DFT band positions has been already confirmed by the comparison with IR spectra, while the full list of Raman activities for the six conformers (for all fundamental bands, overtones and combination bands, reported in the ESI[†]), which allows to simulate the Raman spectra line-shape for any kind of experimental conditions might facilitate further experimental studies on glycine Raman spectra in the whole spectral range.

6 Toward feasible computations for larger molecular systems

For larger systems and/or high numbers of conformers or isopotomers to be considered simultaneously, the computational burden can be significantly scaled down by reduced-dimensionality computations, where the numerical differentiation of analytical Hessian is performed only along some selected normal modes. The latter can be chosen on the basis of spectroscopic observables of interest, for instance the most intense bands in the IR or Raman spectrum, or selected spectral ranges. Recently we have suggested a practical path for reduced-dimensionality VPT2 computations: the sets of normal modes to be considered simultaneously should be selected based on the nature of the vibrations and the related

[†]Electronic Supplementary Information (ESI) available: (*i*) Basis sets from N07D/SNSD family. (*ii*) Best-estimated anharmonic vibrational frequencies and Raman activities for the six conformers of glycine, for all fundamental bands, overtones (2_i) and combination bands (1_i1_j). See DOI: 10.1039/b000000x/

energy range (see Ref.[11] for a detailed analysis). In this way all vibrations mainly localized on the same region of a molecular system (e.g. functional group) and with similar wavenumbers, which are likely to be coupled, are included in the anharmonic treatment. For the Ip conformer of glycine it has been shown[11] that in order to compute the anharmonic wavenumbers of the five high-energy modes with an accuracy comparable to the full dimensional VPT2 treatment it is necessary to include the coupling terms between stretching mode ν_{CH_2as} and both symmetric and asymmetric ν_{NH_2} stretchings. Moreover the best results have been obtained with all five X-H stretching vibrations considered together and with additional inclusion of mode υ_{10}. This approach has been followed in the present work for the simulation of IR and Raman spectra. Figure 10 reports the IR and Raman spectra in the wavenumber ranges related to the X-H stretching fundamental transitions (3600–2800 cm^{-1}) and their overtones and combination bands (7000–5500 cm^{-1}). In all cases, the spectra computed using reduced-dimensionality approaches agree very well with their full VPT2 counterparts, in particular the complex spectral pattern in the fully anharmonic zone of the spectrum (7000–5500 cm^{-1}) is perfectly reproduced by the reduced VPT2 scheme.

The same computational model can be applied to the vibrational study of a hybrid system, for example, glycine adsorbed on a silicon cluster[11,151], allowing to dissect changes of glycine spectra upon adsorption on the Si(100) surface (see Figure 11). In that case, depending on the spectral zone of interest, it is possible to consider only high-energy vibrations for anharmonic computations, as discussed above. Even if all normal modes of glycine are taken into account, the computational cost remains substantially lower with respect to the total system (i.e. the glycine molecule and the substrate, here a $Si_{15}H_{16}$ cluster) with 117 normal modes, for which the determination of full-dimensional anharmonic force-field would require 235 Hessian computations. The reduced-dimensionality VPT2 approach allows to combine the accuracy of the anharmonic treatment with feasible calculations, permitting also a reliable QM description of the associated anharmonic PES. In particular, it is possible to describe both isolated molecule and the whole “molecule+cluster” system at the B3LYP level with double-ζ basis sets. In Figure 11, the five modes with the highest wavenumbers of isolated and adsorbed glycine are compared. It should be noted that the OH stretching is not present in the adsorbed molecule due to the dissociative character of the adsorption process (see reference[151] and references therein), while the Si-H stretching, representative of the new system, is reported. Furthermore, a close similarity of the CH_2 and NH_2 stretching modes has been found between isolated and adsorbed glycine. Extension to even larger systems can be done by combining reduced-dimensionality models with QM/MM schemes[10,105]. We should note that all the approaches discussed above can be also coupled with the description of non-specific environmental effects by means of continuum solvent models[101–103], leading finally to the discrete/continuum representation of complex environments[102,104,105]. A fully coherent polarizable QM/MM/PCM model can be applied to anharmonic computations thanks to the availability of analytical second derivatives with respect to nuclear and electric perturbations[105] and if required combined with reduced-dimensionality VPT2 schemes for the choice of specific degrees of freedom considered for anharmonic computations. Those integrated approaches allow to set up computational procedures tailored for the system and properties under study, including also large systems with localized spectroscopic

phenomena. These strategies have been already shown to provide an improved agreement with experimental results[210–212] for the hybrid organic-inorganic systems such as glycine adsorbed on a silicon cluster as discussed above, or large biomolecules as C=O stretching spectral range for chlorophyll-*a* in a tetrahydrofuran solution[5,11], taking into account both environmental and anharmonic effects, and allowing reinvestigation of experimental outcomes.

7 Improving the accuracy: hybrid approaches

It has been already shown for several small closed- and open-shell molecular systems that the differences between coupled cluster (CC) and DFT anharmonic wavenumbers are mainly due to the harmonic terms[73,82,87–90], paving the route to introduce effective yet reliable hybrid CC/DFT schemes. As a matter of fact, increased accuracy, even for relatively large systems, can be achieved with hybrid approaches where the harmonic part is computed with larger basis sets and/or at higher levels of theory (especially CCSD(T) or double-hybrid B2PLYP), and the anharmonic corrections are evaluated with much less computationally demanding (B3LYP) models. The simplest hybrid approach relies on *a posteriori* DFT corrections to the best estimated harmonic results. Alternatively, the hybrid anharmonic force field can be obtained in a normal-coordinate representation by adding the cubic and semi-diagonal quartic force constants computed at the DFT level to the CC or B2PLYP harmonic wavenumbers within the VPT2 expressions. Since usually the normal modes are very similar, DFT cubic and quartic force constants can be used without any transformation. Such a hybrid anharmonic force field is then used to compute the anharmonic wavenumbers with the VPT2 approach. This procedure, which allows also the anharmonic resonances to be identified based on the more accurate results, and introduces corrections to ω within all VPT2 equations (wavenumbers and intensities) can be advocated as the most reliable and has been used in the present work.

Figure 12 collects results from our recent works[83,91–93,99,147,151,153,160,190], and compares the anharmonic wavenumbers for a set of about 250 fundamental vibrations computed at the B3LYP level, and by hybrid models (where harmonic contributions have been evaluated at the B2PLYP and CCSD(T) levels, with basis sets of at least cc-pVTZ quality) with experimental outcomes. In all cases, anharmonic corrections have been computed at the B3LYP level with, at least, polarized double-ζ basis sets (mainly SNSD/N07D family). This approach provides accurate results for all vibrations except two large-amplitude motions, namely the out-of-plane deformation (υ_2) of NH_3 and the OH stretching involved in an intermolecular hydrogen bond (υ_3) of glycine IIn. First of all, it is further confirmed that B3LYP computations provide, per se, quite reliable anharmonic wavenumbers, with MAEs of 13 cm^{-1}, and maximum discrepancies of about 50 cm^{-1}, in line with the MAE of about 10 cm^{-1} reported for the somehow larger benchmark set in Figure 1. On these grounds, we can safely claim an accuracy of about 10–20 cm^{-1} for B3LYP/SNSD GVPT2 computations. For small-to-medium closed- and open-shell molecular systems, an increased accuracy can be obtained with CC/B3LYP models, which have already been validated for wavenumber computations[73,82,87–90]. Within Coupled Cluster computations, refined harmonic force fields can be evaluated through composite schemes, taking into account extrapolation to the basis set limit, as well as inclusion of core-correlation and diffuse-function corrections.

From a set of molecules adapted for the statistics in Figure 12, the best-estimated CC harmonic wavenumbers have been evaluated for glycine[93,147,190], pyrimidine[91] and uracil[92]. In all other cases CCSD(T) harmonic wavenumbers have been computed in conjunction with basis sets of at least cc-pVTZ quality. The good accuracy of CC/B3LYP wavenumber computation, with an overall MAE well below 10 cm^{-1} and maximum discrepancies not exceeding 30 cm^{-1} is further confirmed, clearly showing that hybrid schemes can deliver wavenumbers of remarkable quality, at computational costs well accessible for medium-sized molecules. As mentioned above, improvements over the B3LYP computations can also be achieved by means of the double-hybrid B2PLYP[145] functional. Computations at the B2PLYP level are significantly more expensive than B3LYP ones, due to the inclusion of second-order perturbation treatment of the electron correlation and larger basis set requirements, but, on the other hand, they can be considered as very cost-effective alternatives with respect to CCSD(T). For this reason, and on the basis of some promising results[85,86,99], we decided to further check the quality of the B2PLYP/B3LYP model. Note that the B2PLYP (and MP2) route suffers from some difficulties for open-shell species since unrestricted approaches require in some cases high-order perturbative terms to reduce spin-contamination at a reasonable level, and restricted open-shell approaches do not include, at low perturbative orders, spin-polarizations effects. From Figure 12, it is evident that the inclusion of B2PLYP harmonic wavenumbers improves results with respect to B3LYP computations, leading sometimes to an agreement close to that issuing from hybrid CC/B3LYP models. Moreover, the improvement is more significant in some difficult cases as for example halo-organic compounds (due to large electronegativities of halogen atoms and, for the heaviest ones, significant relativistic core-electron effects), with a correction of the harmonic terms by means of more accurate methods, either CCSD(T) or B2PLYP/cc-pVTZ(-PP) significantly increasing the wavenumber accuracy. Thus B2PLYP/AVTZ computations of harmonic wavenumbers can be recommended as a viable route to improve the accuracy of anharmonic wavenumbers for relatively large systems. Moreover, hybrid B2PLYP/B3LYP schemes can be advocated as a first choice instead of fully B2PLYP anharmonic computations in all cases where B3LYP wavenumbers yield larger than usual discrepancies. It has been shown that B2PLYP, if coupled to basis sets of at least cc-pVTZ quality, yields harmonic wavenumbers substantially more accurate than other DFT approaches, and in this respect, it outperforms the B3LYP functional[85]. On the other side, the B2PLYP model, if coupled to double-ζ basis sets, does not show any clear improvement for anharmonic force constants over B3LYP. This is explained by the higher basis set requirements related to the second-order perturbation treatment of electron correlation[85]. Table 5 reports harmonic and anharmonic wavenumbers for formic acid computed at B3LYP, B2PLYP/B3LYP and B2PLYP levels, including, for B3LYP, basis set effects (SNSD, SNST and aug-cc-pVTZ). For the formic acid B3LYP computations lead to results which cannot be considered fully satisfactory for the analysis of experimental spectra (maximum discrepancies up to 50 cm^{-1}). In particular, the largest discrepancies are found in the X-H stretchings spectral zone, so for the bands, which are strongly affected (both wavenumbers and intensities) by the creation of formic acid conglomerates. Improved wavenumbers can be obtained by fully anharmonic B2PLYP/AVTZ computations, but results of the same accuracy are also obtained by hybrid B2PLYP/B3LYP models. With respect to the B3LYP computations we note that both harmonic and anharmonic

wavenumbers are essentially converged at the B3LYP/SNSD level, and anharmonic contributions can be safely computed with the least expensive SNSD basis set. However, we also note that for strongly anharmonic modes, improved results can be obtained with anharmonic corrections computed at the B2PLYP/aug-cc-pVTZ level. This is the case of OH stretching mode for glycine IIn/ccc conformer (mode υ_3, not considered in Figure 12) involved in the hydrogen bridge, where CC/B2PLYP and B2PLYP computations halve the deviation from experiment with respect to computations where anharmonic corrections have been obtained at the B3LYP level, albeit at a largely increased computational cost[93].

With respect to intensities, anharmonic hybrid IR intensities and Raman activities have been obtained by means of an *a posteriori* scheme, again assuming that the differences between the two levels of theory can be ascribed only to the harmonic part

$$I_{\text{hybrid}}^{\text{anh}} = I^{\text{harm}}(\text{best}) + \Delta I_{\text{B3LYP}}^{\text{anh}}. \quad (16)$$

Here we consider hybrid schemes with CCSD(T) and B2PLYP levels applied for best-estimated IR intensities, and B2PLYP computations of Raman activities, in all cases in conjunction with basis sets of at least cc-pVTZ quality. Analogously to wavenumbers, a composite scheme can be used to evaluate best-estimates for IR intensities[93,147,161,190]. Regarding the direct comparison with experiment, much less experience is available for IR and, above all, Raman intensities beyond the harmonic level. In this respect, the general implementation presented here is providing encouraging results[5,100]. In particular, B3LYP, B2PLYP and hybrid CC/B3LYP and CC/B2PLYP IR intensities have been compared with experimentally derived integrated cross sections (km mol^{-1}) for a set of halo-organic molecules of atmospheric interest showing in all cases good agreement with experiment even in the spectral ranges due fully to non-fundamental transitions[160]. It has been observed that the agreement between theoretical and experimental intensities is very good already at the B3LYP/SNSD level, with a total MAE of about 7 km mol^{-1}. A slight improvement has been observed by employing B2PLYP/cc-pVTZ(-PP) and B2PLYP/B3LYP computations (MAE of 6 km mol^{-1}), with further improvement reachable with hybrid schemes where the harmonic part is corrected at the CCSD(T) level (MAE of about 2.5 km mol^{-1}). In this regard, it should be pointed out that the B2PLYP or CCSD(T) corrections to wavenumbers are applied to all bands, also including overtones, while the corrections to harmonic intensities influence only the fundamental transitions. However, it is evident that hybrid CC/DFT approaches are useful in order to improve the theoretical intensities. The performance of B3LYP and B2PLYP approaches in predicting IR intensities and Raman activities for formic acid is compared in Tables 6 and 7, respectively. For IR intensities, again B3LYP and B2PLYP yield essentially identical anharmonic corrections, in line with what has been observed for halogenated molecules. Moreover, for B3LYP the anharmonic correction is already converged with the least expensive SNSD basis set, in line with benchmark studies presented in Tables 1-3. On the other hand, improved harmonic IR intensities are obtained by increasing the basis set with the B3LYP functional or with B2PLYP/AVTZ computations. Finally, it is noteworthy that B2PLYP/B3LYP hybrid IR intensities agree within 1 km mol^{-1} with full B2PLYP/AVTZ anharmonic computations. Concerning high-to-medium intensity Raman activities, the B3LYP harmonic contributions

agree within 10 % with their B2PLYP/AVTZ counterparts, while for low-intensity features, discrepancies do not exceed 1 $Å^4$ u^{-1}. Within B3LYP computations both harmonic parts and anharmonic contributions are essentially the same for all basis sets, with the Raman activities for the most intense transitions varying by less than 2.5 $Å^4$ u^{-1}.

The previous analysis leads to some practical considerations for a cost-effective yet reliable simulation of fully anharmonic IR and Raman spectra. First of all, for most of the molecular systems, the accuracy of B3LYP/SNSD computations is fully adequate also for quantitative analyses. For specific cases where even more stringent accuracy is needed, the most viable way to improve the results at a reasonable computational cost goes through hybrid schemes with the harmonic part corrected at CCSD(T) or B2PLYP levels, in conjunction with basis sets of at least cc-pVTZ quality. B2PLYP computations can be advocated for larger systems or in order to reduce the computational cost, still considerable for computation of harmonic wavenumbers at the CCSD(T)/VTZ level even for few-atomic systems. Corrections of harmonic contributions are more important for wavenumbers than for intensities, at least for the interpretation of experimental outcomes and unless high-quality quantitative data for transition intensities are required. It should be noted that the correction of band position influences the pattern of simulated transitions, hence the overall spectral line-shape. For some difficult cases, involving strongly anharmonic PES or challenging description of the electronic structure, improved anharmonic corrections can be computed at the B2PLYP/AVTZ level.

This strategy has been applied to simulate IR and Raman spectra of formic acid and its complexes, which are concomitantly present under experimental conditions in low-temperature Argon matrices[213–215]. Formation of weakly bound molecular systems in matrix environments requires the proper consideration of all the most probable aggregates, with simultaneous measurements of IR and Raman spectra significantly facilitating the analysis of experimental outcomes[213–216]. Here, we show that spectra of such mixture can be directly simulated at a fully anharmonic level allowing a *vis-à-vis* comparison with its experimental counterpart. In the case of the formic acid monomer, improved anharmonic wavenumbers have been obtained with B2PLYP/AVTZ and hybrid B2PLYP/B3LYP computations. For the simulation of the spectra of the monomer and dimers, we resort to the less expensive one between those approaches, i.e. the hybrid B2PLYP/B3LYP model with anharmonic corrections computed at the B3LYP/SNSD level. Figure 13 compares the simulated spectra of the monomer, the two most stable dimers[215] and a mixture of all the species with the experimental IR and Raman spectra[214,215]. In this case, the Raman spectra have been reported directly in terms of scattering intensities, without any scaling. For this reason, we have computed the corresponding theoretical values according to Equation 8 starting from anharmonic Raman activities in $Å^4$ u^{-1} and considering an excitation wavenumber equal to 18797 cm^{-1} (532 nm)[215]. According to the different concentration of formic acid in Ar matrix for both experiments and the higher stability of the cyclic dimers we have adopted a 5-30% interval for the dimer contribution to the overall spectra. Figure 13 shows a very good agreement between simulated and experimental IR and Raman spectra, considering both the band positions and the intensity patterns. In particular, it is evident that several new features emerging with respect to the monomer spectra, can be

assigned to one of the dimers. This example highlights the accuracy and feasibility of fully anharmonic simulations of IR and Raman spectra for complex molecular mixtures.

8 Conclusions and Future Developments

We have discussed our general approach and analysed some representative results for the description of vibrational spectra for isolated molecules (gas phase, low-temperature matrices, nanodroplets) with the contemporary account of mechanical and electrical anharmonicity. The computational approach and the general trends, even if here applied to few small-to-medium sized systems, should not be considered as specific of given molecular structures, but as an account of the present situation of a much wider general project. The implementation of the whole approach in a widely available and user-friendly suite of programs allows the use of all quantum mechanical methods for which analytical second derivatives of energies and analytical first derivatives of electric properties are available: numerical differentiation of all these terms provides the quantities needed for the evaluation of anharmonic vibrational wavenumbers and intensities. Comparison of the calculated results with their experimental counterparts suggests that remarkably accurate anharmonic contributions can be obtained by quite inexpensive basis sets and QM methods, thus allowing to concentrate computational efforts on the harmonic terms, whose convergence with the many-body contributions and/or basis set extension are more demanding. The quality of the results obtained by this new robust black-box procedures for the proper inclusion of resonance effects shows that VPT2 is the method of choice for the study of low-energy spectra (i.e. including fundamentals together with first overtones and combination bands) of medium and large-size semirigid molecules in the gas phase. Even larger systems can be accurately studied employing reduced-dimensionality approaches, which allow the inclusion of diagonal anharmonicity only for a selected and tunable number of normal modes, but including the most important anharmonic couplings also with inactive modes. Although true large amplitude motions are still problematic, the ongoing development of approaches based on internal coordinates promises to further extend the range of application of VPT2. It is, of course, always possible to resort to mixed variational/perturbative approaches, but then the true problem becomes the definition and evaluation of a reliable potential energy surface going beyond the fourth-order polynomial approximation. In our opinion pathways to go beyond the VPT2 scheme should be rather explored for specific/necessary cases only, and we preferred to highlight the applicability and accuracy of the present VPT2 model. Another issue concerns the treatment of systems in condensed phase. Here the polarizable continuum model (PCM) has been already extended to wavenumbers and IR intensities with promising results and the corresponding developments for Raman spectra are in a final stage of testing. Of course, explicit solvent molecules need to be included whenever specific effects in the cybotactic region are important. Here again, ongoing work based on mixed discrete/continuum models and/or integration of time-independent and time-dependent approaches is giving promising results. In conclusion, the results reported in this perspective and in the underlying specific studies show, in our opinion, that despite pending further developments, we dispose *"hic and nunc"* of a powerful general tool (which can be referred to as a first generation multifrequency virtual

Europe PMC Funders Author Manuscripts

spectrometer) for complementing and aiding vibrational studies for molecular systems of current scientific and technological interest.

Supplementary Material

Refer to Web version on PubMed Central for supplementary material.

Acknowledgements

The research leading to these results has received funding from the European Union's Seventh Framework Programme (FP7/2007-2013) under grant agreement N^{O} ERC-2012-AdG-320951-DREAMS. The high performance computer facilities of the DREAMS center (http://dreamshpc.sns.it) are acknowledged for providing computer resources. The support of COST CMTS-Action CM1002 "COnvergent Distributed Environment for Computational Spectroscopy (CODECS)" is also acknowledged. The authors thank Dr. Adriana Olbert-Majkut for providing the experimental data of IR and Raman spectroscopic measurements of formic acid. Prof. C. Puzzarini, Prof. C. Cappelli, I. Carnimeo, F. Egidi and P. Panek are acknowledged for their contribution to the results presented in this work and/or valuable comments.

References

1. Siebert, F.; Hildebrandt, P., editors. Vibrational Spectroscopy in Life Science. Wiley-VCH Verlag GmbH and Co. KGaA; 2008.
2. Barth A, Zscherp C. Quarterly Reviews of Biophysics. 2002; 35:369–430. [PubMed: 12621861]
3. Laane, J., editor. Frontiers of Molecular Spectroscopy. Elsevier; Amsterdam: 2009.
4. Quack, M.; Merkt, F. Handbook of High-Resolution Spectroscopy. John Wiley & Sons; 2011.
5. Barone V, Baiardi A, Biczysko M, Bloino J, Cappelli C, Lipparini F. Phys. Chem. Chem. Phys. 2012; 14:12404–12422. [PubMed: 22772710]
6. Barone, V., editor. Computational Strategies for Spectroscopy, from Small Molecules to Nano Systems. John Wiley & Sons, Inc.; Hoboken, New Jersey: 2011.
7. Grunenberg, J., editor. Computational Spectroscopy. Wiley-VCH Verlag GmbH & Co. KGaA; 2010.
8. Herrmann, C.; Reiher, M. Atomistic Approaches in Modern Biology: from Quantum Chemistry to Molecular Simulations. Reiher, M., editor. Vol. 268. Springer-Verlag; Berlin, Germany: 2007. p. 85-132.
9. Pedone A, Biczysko M, Barone V. Chem. Phys. Chem. 2010; 11:1812–1832. [PubMed: 20358575]
10. Barone V, Biczysko M, Brancato G. Adv. Quantum Chem. 2010; 59:17.
11. Barone V, Biczysko M, Bloino J, Borkowska-Panek M, Carnimeo I, Panek P. Int. J. Quantum Chem. 2012; 112:2185–2200.
12. Neugebauer J, Reiher M, Kind C, Hess BA. J. Comput. Chem. 2002; 23:895–910. [PubMed: 11984851]
13. Herrmann C, Neugebauer J, Reiher M. New J. Chem. 2007; 31:818–831.
14. Jacob CR, Luber S, Reiher M. J. Phys. Chem. B. 2009; 113:6558–6573. [PubMed: 19361178]
15. Cappelli, C.; Biczysko, M. ch. Time-Independent Approach to Vibrational Spectroscopies. In: Barone, V., editor. Computational Strategies for Spectroscopy, from Small Molecules to Nano Systems. John Wiley & Sons, Inc.; 2011. p. 309-360.
16. Jensen, P.; Bunker, PR. Computational Molecular Spectroscopy. John Wiley and Sons Ltd; Chichester, UK: 2000.
17. Császár AG. WIREs Comput. Mol. Sci. 2012; 2:273289.
18. Rizzo, A.; Coriani, S.; Ruud, K. ch. Response Function Theory Computational Approaches to Linear and Nonlinear Optical Spectroscopy. In: Barone, V., editor. Computational Strategies for Spectroscopy, from Small Molecules to Nano Systems. John Wiley & Sons, Inc.; 2011. p. 77-135.
19. Helgaker T, Coriani S, Jørgensen P, Kristensen K, Olsen J, Ruud K. Chem. Rev. 2012; 112:543–631. [PubMed: 22236047]

20. Bowman JM, Carrington T, Meyer H-D. Mol. Phys. 2008; 106:2145–2182.
21. Pesonen, J.; Halonen, L. Adv. Chem. Phys. Vol. 125. John Wiley Sons, Inc.; 2003. ch. Recent Advances in the Theory of Vibration-Rotation Hamiltonians; p. 269-349.
22. Császár AG, Fabri C, Szidarovszky T, Matyus E, Furtenbacher T, Czako G. Phys. Chem. Chem. Phys. 2012; 14:1085–1106. [PubMed: 21997300]
23. Tennyson J. WIREs Comput. Mol. Sci. 2012; 2:698–715.
24. Puzzarini C, Stanton JF, Gauss J. Int. Rev. Phys. Chem. 2010; 29:273–367.
25. Carrington T, Wang X-G. WIREs Comput. Mol. Sci. 2011; 1:952–963.
26. Rauhut G, Pulay P. J. Phys. Chem. 1995; 99:3093–3100.
27. Sinha P, Boesch SE, Gu C, Wheeler RA, Wilson AK. J. Phys. Chem. A. 2004; 108:9213–9217.
28. Andersson MP, Uvdal PE. J. Phys. Chem. A. 2005; 109:2937–2941. [PubMed: 16833612]
29. Teixeira F, Melo A, Cordeiro MNDS. J. Chem. Phys. 2010; 133:114109. [PubMed: 20866128]
30. Alecu IM, Zheng J, Zhao Y, Truhlar DG. J. Chem. Theory Comput. 2010; 6:2872–2887.
31. Katsyuba SA, Zvereva EE, Burganov TI. J. Phys. Chem. A. 2013; 117:6664–6670. [PubMed: 23805975]
32. Baker J, Jarzecki AA, Pulay P. J. Phys. Chem. A. 1998; 102:1412–1424.
33. Fabri C, Szidarovszky T, Magyarfalvi G, Tarczay G. J. Phys. Chem. A. 2011; 115:4640–4649. [PubMed: 21495661]
34. Barone V, Improta R, Rega N. Accounts of Chemical Research. 2008; 41:605–616. [PubMed: 18307319]
35. Miani A, Helfand MS, Raugei S. J. Chem. Theory Comput. 2009; 5:2158–2172.
36. Gaigeot M-P, Besley NA, Hirst JD. J. Phys. Chem. B. 2011; 115:5526–5535. [PubMed: 21344909]
37. Kirchner, B.; Dio, P.; Hutter, J. Multiscale Molecular Methods in Applied Chemistry. Kirchner, B.; Vrabec, J., editors. Vol. 307. Springer; Berlin Heidelberg: 2012. p. 109-153.
38. Thomas M, Brehm M, Fligg R, Vohringer P, Kirchner B. Phys. Chem. Chem. Phys. 2013; 15:6608–6622. [PubMed: 23416970]
39. Mills, IM. Molecular Spectroscopy: Modern Research. Academic; New York: 1972.
40. Truhlar DG, Olson RW, Jeannotte AC, Overend J. J. Am. Chem. Soc. 1976; 98:2373–2379.
41. Isaacson AD, Truhlar DG, Scanlon K, Overend J. J. Chem. Phys. 1981; 75:3017–3024.
42. Clabo DA Jr. Allen WD, Remington RB, Yamaguchi Y, Schaefer HF III. Chem. Phys. 1988; 123:187–239.
43. Allen WD, Yamaguchi Y, Császár AG, Clabo DA Jr. Remington RB, Schaefer HF III. Chem. Phys. 1990; 145:427–466.
44. Amos RD, Handy NC, Green WH, Jayatilaka D, Willets A, Palmieri P. J. Chem. Phys. 1991; 95:8323–8336.
45. Maslen PE, Handy NC, Amos RD, Jayatilaka D. J. Chem. Phys. 1992; 97:4233–4254.
46. Gaw, F.; Willetts, A.; Handy, N.; Green, W. SPEC-TRO - a program for derivation of spectroscopic constants from provided quartic force fields and cubic dipole fields. Bowman, JM., editor. Vol. 1B. JAI Press; 1991. p. 169-185.
47. Zhang Q, Day PN, Truhlar DG. J. Chem. Phys. 1993; 98:4948–4958.
48. Barone V. J. Chem. Phys. 1994; 101:10666–10676.
49. Barone V. J. Chem. Phys. 2005; 122:014108.
50. Barone V. J. Chem. Phys. 2004; 120:3059–3065. [PubMed: 15268458]
51. Gaw, F.; Willetts, A.; Handy, N.; Green, W. Advances in Molecular Vibrations and Collision Dynamics. Bowman, JM., editor. Vol. 1B. 1991. p. 169-185.
52. Martin JML, Lee TJ, Taylor PM, François J-P. J. Chem. Phys. 1995; 103:2589–2602.
53. Stanton JF, Gauss J. J. Chem. Phys. 1998; 108:9218–9220.
54. Ruden TA, Taylor PR, Helgaker T. J. Chem. Phys. 2003; 119:1951–1960.
55. Ruud K, Åstrand PO, Taylor PR. J. Chem. Phys. 2000; 112:2668–2683.
56. Stanton JF, Gauss J. Int. Rev. Phys. Chem. 2000; 19:61–95.
57. Neugebauer J, Hess BA. J. Chem. Phys. 2003; 118:7215–7225.

58. Vázquez J, Stanton JF. Mol. Phys. 2006; 104:377–388.
59. Vázquez J, Stanton JF. Mol. Phys. 2007; 105:101–109.
60. Carbonniere P, Dargelos A, Pouchan C. Theoret. Chim. Acta. 2010; 125:543.
61. Hermes MR, Hirata S. J. Chem. Phys. 2013; 139:034111. [PubMed: 23883014]
62. Bowman JM. Science. 2000; 290:724–725. [PubMed: 11184203]
63. Roy TK, Gerber RB. Phys. Chem. Chem. Phys. 2013; 15:9468–9492. [PubMed: 23677257]
64. Bowman JM, Carter S, Huang X. Int. Rev. Phys. Chem. 2003; 22:533–549.
65. Carter S, Handy N. J. Chem. Phys. 2000; 113:987–993.
66. Carter S, Sharma AR, Bowman JM, Rosmus P, Tarroni R. J. Chem. Phys. 2009; 131:224106. [PubMed: 20001023]
67. Chaban GM, Jung JO, Gerber RB. J. Chem. Phys. 1999; 111:1823–1829.
68. Rauhut G, Hrenar T. Chem. Phys. 2008; 346:160–166.
69. Christiansen O. Phys. Chem. Chem. Phys. 2007; 9:2942–2953. [PubMed: 17551617]
70. Norris LS, Ratner MA, Roitberg AE, Gerber RB. J. Chem. Phys. 1996; 105:11261–11268.
71. Christiansen O. J. Chem. Phys. 2003; 119:5773–5781.
72. Cassam-Chenai P, Lievin J. J. Comput. Chem. 2006; 27:627–640. [PubMed: 16470836]
73. Carbonniere P, Lucca T, Pouchan C, Rega N, Barone V. J. Comput. Chem. 2005; 26:384–388. [PubMed: 15651031]
74. Barone V. Chem. Phys. Lett. 2004; 383:528–532.
75. Miani A, Cane E, Palmieri P, Trombetti A, Handy NC. J. Chem. Phys. 2000; 112:248–259.
76. Barone V. J. Phys. Chem. A. 2004; 108:4146–4150.
77. Burcl R, Handy NC, Carter S. Spectrochim. Acta A. 2003; 59:1881–1893.
78. Burcl R, Carter S, Handy NC. Phys. Chem. Chem. Phys. 2004; 6:340–343.
79. Boese AD, Martin J. J. Phys. Chem. A. 2004; 108:3085–3096.
80. Cane E, Miani A, Trombetti A. J. Phys. Chem. A. 2007; 111:8218–8222. [PubMed: 17672437]
81. Barone V, Bloino J, Biczysko M. Phys. Chem. Chem. Phys. 2010; 12:1092–1101. [PubMed: 20094674]
82. Puzzarini C, Biczysko M, Barone V. J. Chem. Theory Comput. 2010; 6:828–838.
83. Bloino J, Biczysko M, Barone V. J. Chem. Theory Comput. 2012; 8:1015–1036.
84. Neese F, Schwabe T, Grimme S. J. Chem. Phys. 2007; 126:124115/1–15. [PubMed: 17411116]
85. Biczysko M, Panek P, Scalmani G, Bloino J, Barone V. J. Chem. Theory Comput. 2010; 6:2115–2125.
86. Kozuch S, Gruzman D, Martin JML. J. Phys. and Colloid Chem. 2010; 114:20801–20808.
87. Puzzarini C, Barone V. J. Chem. Phys. 2008; 129:084306/1–7. [PubMed: 19044822]
88. Puzzarini C, Barone V. Phys. Chem. Chem. Phys. 2008; 10:6991–6997. [PubMed: 19030595]
89. Begue D, Carbonniere P, Pouchan C. J. Phys. Chem. A. 2005; 109:4611–4616. [PubMed: 16833799]
90. Begue D, Benidar A, Pouchan C. Chem. Phys. Lett. 2006; 430:215–220.
91. Biczysko M, Bloino J, Brancato G, Cacelli I, Cappelli C, Ferretti A, Lami A, Monti S, Pedone A, Prampolini G, Puzzarini C, Santoro F, Trani F, Villani G. Theoret. Chim. Acta. 2012; 131:1201.
92. Puzzarini C, Biczysko M, Barone V. J. Chem. Theory Comput. 2011; 7:3702–3710.
93. Barone V, Biczysko M, Bloino J, Puzzarini C. Phys. Chem. Chem. Phys. 2013; 15:10094–10111. [PubMed: 23599122]
94. Assfeld X, Almlöf JE, Truhlar DG. Chem. Phys. Lett. 1995; 241:438–444.
95. Kuhler KM, Truhlar DG, Isaacson AD. J. Chem. Phys. 1996; 104:4664–4671.
96. Krasnoshchekov SV, Isayeva EV, Stepanov NF. J. Phys. Chem. A. 2012; 116:3691–3709. [PubMed: 22369280]
97. Bludský O, Bak KL, Jørgensen P, Špirko V. J. Chem. Phys. 1995; 103:10110–10115.
98. Barone V, Bloino J, Guido CA, Lipparini F. Chem. Phys. Lett. 2010; 496:157–161.
99. Biczysko M, Bloino J, Carnimeo I, Panek P, Barone V. J. Mol. Spectrosc. 2012; 1009:74–82.

100. Bloino J, Barone V. J. Chem. Phys. 2012; 136:124108. [PubMed: 22462836]
101. Cappelli C, Lipparini F, Bloino J, Barone V. J. Chem. Phys. 2011; 135:104505. [PubMed: 21932908]
102. Cappelli C, Bloino J, Lipparini F, Barone V. J. Phys. Chem. Lett. 2012; 3:1766–1773. [PubMed: 26291857]
103. Egidi F, Bloino J, Cappelli C, Barone V. Chirality. 2013 DOI:10.1002/chir.22200.
104. Scalmani G, Barone V, Kudin K, Pomelli C, Scuseria G, Frisch M. Theor. Chem. Acc. 2004; 111:90.
105. Lipparini F, Cappelli C, Scalmani G, De Mitri N, Barone V. J. Chem. Theory Comput. 2012; 8:4270–4278.
106. Rega N, Brancato G, Petrone A, Caruso P, Barone V. J. Chem. Phys. 2011; 134:074504. [PubMed: 21341856]
107. Barone V, Cimino P, Stendardo E. J. Chem. Theory Comput. 2008; 4:751.
108. Barone V, Cimino P. Chem. Phys. Lett. 2008; 454:139–143.
109. Barone V, Cimino P. J. Chem. Theory Comput. 2009; 5:192–199.
110. Pavone M, Rega N, Barone V. Chem. Phys. Lett. 2008; 452:333–339.
111. [accessed February 1, 2013] Double and triple-ζ basis sets of SNS and N07 families, are available for download. 2012. visit http://dreamslab.sns.it
112. Nielsen HH. Reviews of Modern Physics. 1951; 23:90–136.
113. Isaacson AD, Truhlar DG, Scanlon K, Overend J. J. Chem. Phys. 1981; 75:3017–3024.
114. Vázquez J, Stanton JF. Mol. Phys. 2006; 104:377–388.
115. Bloino J, Biczysko M, Barone V. J. Chem. Theory Comput. 2012; 8:1015–1036.
116. Barone V, Festa G, Grandi A, Rega N, Sanna N. Chem. Phys. Lett. 2004; 388:279–283.
117. Biczysko M, Panek P, Barone V. Chem. Phys. Lett. 2009; 475:105–110.
118. Hirata S, Yagi K. Chem. Phys. Lett. 2008; 464:123–134.
119. Bouř P. J. Phys. Chem. 1994; 98:8862–8865.
120. Faulkner TR, Marcott C, Moscowitz A, Overend J. J. Am. Chem. Soc. 1977; 99:8160–8168.
121. Miller WH, Hernandez R, Handy NC, Jayatilaka D, Willets A. Chem. Phys. Lett. 1990; 172:62–68.
122. Truhlar DG, Isaacson AD. J. Chem. Phys. 1991; 94:357–359.
123. Schuurman MS, Allen WD, von Ragué Schleyer P, Schaefer HF III. J. Chem. Phys. 2005; 122:104302. [PubMed: 15836311]
124. Ayala PY, Schlegel HB. J. Phys. Chem. 1998; 108:2314–2325.
125. McClurg RB, Flagan RC, Goddard WA III. J. Chem. Phys. 1997; 106:6675–6680.
126. McClurg RB. J. Chem. Phys. 1999; 111:7165–7165.
127. McClurg RB. J. Chem. Phys. 1999; 111:7163–7164.
128. Truhlar DG. J. Comput. Chem. 1991; 12:266–270.
129. Chuang Y-Y, Truhlar DG. J. Chem. Phys. 2000; 112:1221–1228.
130. Strekalov M. Chem. Phys. 2009; 362:75–81.
131. Zheng J, Yu T, Papajak E, Alecu IM, Mielke SL, Truhlar DG. Phys. Chem. Chem. Phys. 2011; 13:10885–10907. [PubMed: 21562655]
132. Zheng J, Truhlar DG. J. Chem. Theory Comput. 2013; 9:2875–2881.
133. Frisch, MJ.; Trucks, GW.; Schlegel, HB.; Scuseria, GE.; Robb, MA.; Cheeseman, JR.; Scalmani, G.; Barone, V.; Mennucci, B.; Petersson, GA.; Nakatsuji, H.; Caricato, M.; Li, X.; Hratchian, HR.; Izmaylov, AF.; Bloino, J.; Zheng, G.; Sonnenberg, JL.; Hada, M.; Ehara, M.; Toyota, K.; Fukuda, R.; Hasegawa, J.; Ishida, M.; Nakajima, T.; Honda, Y.; Kitao, O.; Nakai, H.; Vreven, T.; Montgomery, JR., Jr.; Peralta, JA.; Ogliaro, F.; Bearpark, M.; Heyd, JJ.; Brothers, E.; Kudin, KN.; Staroverov, VN.; Kobayashi, R.; Normand, J.; Raghavachari, K.; Rendell, A.; Burant, JC.; Iyengar, SS.; Tomasi, J.; Cossi, M.; Rega, N.; Millam, JM.; Klene, M.; Knox, JE.; Cross, JB.; Bakken, V.; Adamo, C.; Jaramillo, J.; Gomperts, R.; Stratmann, RE.; Yazyev, O.; Austin, R.; J., A.; Cammi; Pomelli, C.; Ochterski, JW.; Martin, RL.; Morokuma, K.; Zakrzewski, VG.; Voth,

GA.; Salvador, P.; Dannenberg, JJ.; Dapprich, S.; Daniels, AD.; Farkas, O.; Foresman, JB.; Ortiz, JV.; Cioslowski, J.; Fox, DJ. Gaussian 09 Revision D.01. Gaussian Inc.; Wallingford CT: 2013. 2009

134. Becke D. J. Chem. Phys. 1993; 98:5648–5652.
135. Yanai T, Tew DP, Handy NC. Chem. Phys. Lett. 2004; 393:51–57.
136. Adamo C, Barone V. J. Chem. Phys. 1999; 110:6158–6170.
137. Jacquemin D, Perpète E, Scalmani G, Frisch MJ, Kobayashi R, Adamo C. J. Chem. Phys. 2007; 126:144105–1. [PubMed: 17444699]
138. Zhao Y, Schults NE, Truhlar DG. J. Chem. Theory Comput. 2006; 2:364–382.
139. Zhao Y, Truhlar DG. Theoret. Chim. Acta. 2008; 120:215–241.
140. Henderson T, Izmaylov AF, Scalmani G, Scuseria GE. J. Chem. Phys. 2009; 131:044108–1. [PubMed: 19655838]
141. Hamprecht FA, Cohen A, Tozer DJ, Handy NC. J. Chem. Phys. 1998; 109:6264–6271.
142. Chai J-D, Head-Gordon M. J. Chem. Phys. 2008; 128:084106/1–15. [PubMed: 18315032]
143. Grimme S. J. Comput. Chem. 2006; 27:1787–1799. [PubMed: 16955487]
144. Chai J-D, Head-Gordon M. Phys. Chem. Chem. Phys. 2008; 10:6615–6620. [PubMed: 18989472]
145. Grimme S. J. Chem. Phys. 2006; 124:034108. [PubMed: 16438568]
146. Schwabe T, Grimme S. Phys. Chem. Chem. Phys. 2007; 9:3397–3406. [PubMed: 17664963]
147. Barone V, Biczysko M, Bloino J, Puzzarini C. J. Chem. Theory Comput. 2013; 9:1533–1547.
148. Grimme S, Antony J, Ehrlich S, Krieg H. J. Chem. Phys. 2010; 132:154104. [PubMed: 20423165]
149. Fornaro, T.; Monti, S.; Biczysko, M.; Barone, V. In preparation
150. Becke AD. J. Chem. Phys. 1993; 98:5648.
151. Carnimeo I, Biczysko M, Bloino J, Barone V. Phys. Chem. Chem. Phys. 2011; 13:16713–16727. [PubMed: 21858336]
152. Bloino J, Biczysko M, Santoro F, Barone V. J. Chem. Theory Comput. 2010; 6:1256–1274.
153. Barone V, Biczysko M, Bloino J, Egidi F, Puzzarini C. J. Chem. Phys. 2013; 138:234303. [PubMed: 23802956]
154. Halls MD, Schlegel HB. J. Chem. Phys. 1998; 109:10587–10593.
155. Halls MD, Schlegel HB. J. Chem. Phys. 1999; 111:8819–8824.
156. Galabov B, Yamaguchi Y, Remington RB, Schaefer HF. J. Phys. Chem. A. 2002; 106:819–832.
157. Thomas JR, DeLeeuw BJ, Vacek G, Crawford TD, Yamaguchi Y, Schaefer HF III. J. Chem. Phys. 1993; 99:403–412.
158. Galabov, B.; Dudev, T. Vibrational Intensities. Elsevier Science; Amsterdam: 1996.
159. Cheeseman JR, Frisch MJ. J. Chem. Theory Comput. 2011; 7:3323–3334.
160. Carnimeo I, Puzzarini C, Tasinato N, Stoppa P, Charmet AP, Biczysko M, Cappelli C, Barone V. J. Chem. Phys. 2013; 139:074310. [PubMed: 23968095]
161. Puzzarini C, Biczysko M, Barone V. J. Chem. Theory Comput. 2011; 7:3702–3710.
162. Charmet AP, Stoppa P, Tasinato N, Giorgianni S, Barone V, Biczysko M, Bloino J, Cappelli C, Carnimeo I, Puzzarini C. J. Chem. Phys. 2013; 139 just accepted.
163. Sadlej A. Theoret. Chim. Acta. 1992; 79:123.
164. Dunning TH. J. Chem. Phys. 1989; 90:1007.
165. Kendall RA, Dunning J. Thom H. Harrison RJ. J. Chem. Phys. 1992; 96:6796.
166. Jimenez-Hoyos CA, Janesko BG, S. GE. Phys. Chem. Chem. Phys. 2008; 10:6621. [PubMed: 18989473]
167. Zvereva EE, Shagidullin AR, Katsyuba SA. J. Phys. Chem. A. 2011; 115:63–69. [PubMed: 21142133]
168. Oakes R, Bell S, Benkova Z, Sadlej A. J. Comput. Chem. 2005; 26:154–159. [PubMed: 15584075]
169. Joshi SP, Dutta AK, Pal S, Vaval N. Chem. Phys. 2012; 403:25–32.
170. Vidal L, Vazquez P. Theoret. Chim. Acta. 2012; 131:1111/1–8.

171. Williams S, Johnson T, Gibbons T, Kitchens C. Theoret. Chim. Acta. 2007; 117:283–290.
172. Hendra, P.; Jones, C.; Warnes, G. Fourier Transform Raman Spectroscopy. Ellis Horwood Ltd; Chichester: 1991.
173. Szczepaniak K, Szczesniak MM, Person WB. J. Phys. Chem. A. 2000; 104:3852–3863.
174. Forbes, MDE., editor. Carbon-Centered Free Radicals and Radical Cations. John Willey & Sons, Inc.; 2010.
175. Radziszewski J. Chem. Phys. Lett. 1999; 301:565–570.
176. Biczysko M, Bloino J, Barone V. Chem. Phys. Lett. 2009; 471:143–147.
177. Sattelmeyer KW, Schaefer HF III. J. Chem. Phys. 2002; 117:7914–7416.
178. Letendre J, Liu D-K, Pibel CD, Halpern JB. J. Chem. Phys. 2000; 112:9209.
179. Sharma AR, Braams BJ, Carter S, Shepler BC, Bowman JM. J. Chem. Phys. 2009; 130:174301/1–9. [PubMed: 19425770]
180. Nikow M, Wilhelm MJ, Dai H-L. J. Phys. Chem. A. 2009; 113:8857–8870. [PubMed: 19594157]
181. Friderichsen AV, Radziszewski JG, Nimlos MR, Winter PR, Dayton DC, David DE, Ellison GB. J. Am. Chem. Soc. 2001; 123:1977–1988. [PubMed: 11456819]
182. Lapinski A, Spanget-Larsen J, Langgard M, Waluk J, Radziszewski GJ. J. Phys. Chem. A. 2001; 105:10520.
183. Karton A, Rabinovich E, Martin JML, Ruscic B. J. Chem. Phys. 2006; 125:144108. [PubMed: 17042580]
184. Karton A, Taylor PR, Martin JML. J. Chem. Phys. 2007; 127:064104. [PubMed: 17705585]
185. Karton A, Daon S, Martin JM. Chem. Phys. Lett. 2011; 510:165–178.
186. Tajti A, Szalay PG, Császár AG, Kallay M, Gauss J, Valeev EF, Flowers BA, Vázquez J, Stanton JF. J. Chem. Phys. 2004; 121:11599–11613. [PubMed: 15634125]
187. Bomble YJ, Vazquez J, Kallay M, Michauk C, Szalay PG, Cszszar AG, Gauss J, Stanton JF. J. Chem. Phys. 2006; 125:064108.
188. Harding ME, Vazquez J, Ruscic B, Wilson AK, Gauss J, Stanton JF. J. Chem. Phys. 2008; 128:114111. [PubMed: 18361558]
189. Karton A, Ruscic B, Martin JM. J. Mol. Struct. Theochem. 2007; 811:345–353.
190. Barone V, Biczysko M, Bloino J, Puzzarini C. Phys. Chem. Chem. Phys. 2013; 15:1358–1363. [PubMed: 23247893]
191. Barna D, Nagy B, Csontos J, Császár AG, Tasi G. J. Chem. Theory Comput. 2012; 8:479–486.
192. [Last accessed February 2nd 2013] see http://webbook.nist.gov/cgi/cbook.cgi?ID=C106978Type=IR-SPECIndex=21IR-SPEC
193. Durig J, Wang A, Beshir W, Littke T. J. Raman Spectrosc. 1991; 22:683–704.
194. Pele L, Sebek J, Potma EO, Gerber RB. Chem. Phys. Lett. 2011; 515:7–12.
195. Yagi K, Taketsugu T, Hirao K, Gordon MS. J. Chem. Phys. 2000; 113:1005.
196. Godfrey PD, Brown RD. J. Am. Chem. Soc. 1995; 117:2019–2023.
197. Suenram RD, Lovas FJ. J. Am. Chem. Soc. 1980; 102:7180–7184.
198. Iijima K, Tanaka K, Onuma S. J. Molec. Structure. 1991; 246:257–266.
199. McGlone S, Elmes P, Brown R, Godfrey P. J. Mol. Spectrosc. 1999; 485 - 486:225–238.
200. Alonso J, Cocinero E, Lesarri A, Sanz M, Lopez J. Angew. Chem. Int. Ed. 2006; 45:3471–3474.
201. Espinoza C, Szczepanski J, Vala M, Polfer NC. J. Phys. Chem. A. 2010; 114:5919–5927. [PubMed: 20405902]
202. Linder R, Seefeld K, Vavra A, Kleinermanns K. Chem. Phys. Lett. 2008; 453:1–6.
203. Balabin RM. J. Phys. Chem. Lett. 2010; 1:20–23.
204. Balabin RM. Phys. Chem. Chem. Phys. 2012; 14:99–103. [PubMed: 21842081]
205. Stepanian SG, Reva ID, Radchenko ED, Rosado MTS, Duarte MLTS, Fausto R, Adamowicz L. J. Phys. Chem. A. 1998; 102:1041–1054.
206. Ivanov A, Sheina G, Blagoi Y. Spectrochim. Acta A. 1998; 55:219–228.
207. Bazso G, Magyarfalvi G, Tarczay G. J. Molec. Structure. 2012; 1025:33–42.

208. Bazso G, Magyarfalvi G, Tarczay G. J. Phys. Chem. A. 2012; 116:10539–10547. [PubMed: 23061476]
209. Huisken F, Werhahn O, Ivanov AY, Krasnokutski SA. J. Chem. Phys. 1999; 111:2978–2984.
210. Lopez A, Heller T, Bitzer T, Richardson N. Chem. Phys. 2002; 277:1.
211. Wang R, Parameswaran S, Hastings G. Vib. Spectrosc. 2007; 44:357.
212. Parameswaran S, Wang R, Hastings G. J. Phys. Chem. B. 2008; 112:14056. [PubMed: 18842020]
213. Reva I, Plokhotnichenko A, Radchenko E, Sheina G, Blagoyi Y. Spectrochim. Acta A. 1994; 50:1107–1111.
214. Macoas EM, Lundell J, Pettersson M, Khriachtchev L, Fausto R, Rasanen M. J. Mol. Spectrosc. 2003; 219:70–80.
215. Olbert-Majkut A, Ahokas J, Lundell J, Pettersson M. Chem. Phys. Lett. 2009; 468:176–183.
216. Olbert-Majkut A, Ahokas J, Lundell J, Pettersson M. J. Raman Spectrosc. 2011; 42:1670–1681.
217. Bertie JE, Michaelian KH. J. Chem. Phys. 1982; 76:886–894.
218. Hisatsun I, Heicklen J. Can. J. Spectrosc. 1973; 18:135–142.
219. Bloino J, Biczysko M, Crescenzi O, Barone V. J. Chem. Phys. 2008; 128:244105. [PubMed: 18601315]

Europe PMC Funders Author Manuscripts

Europe PMC Funders Author Manuscripts

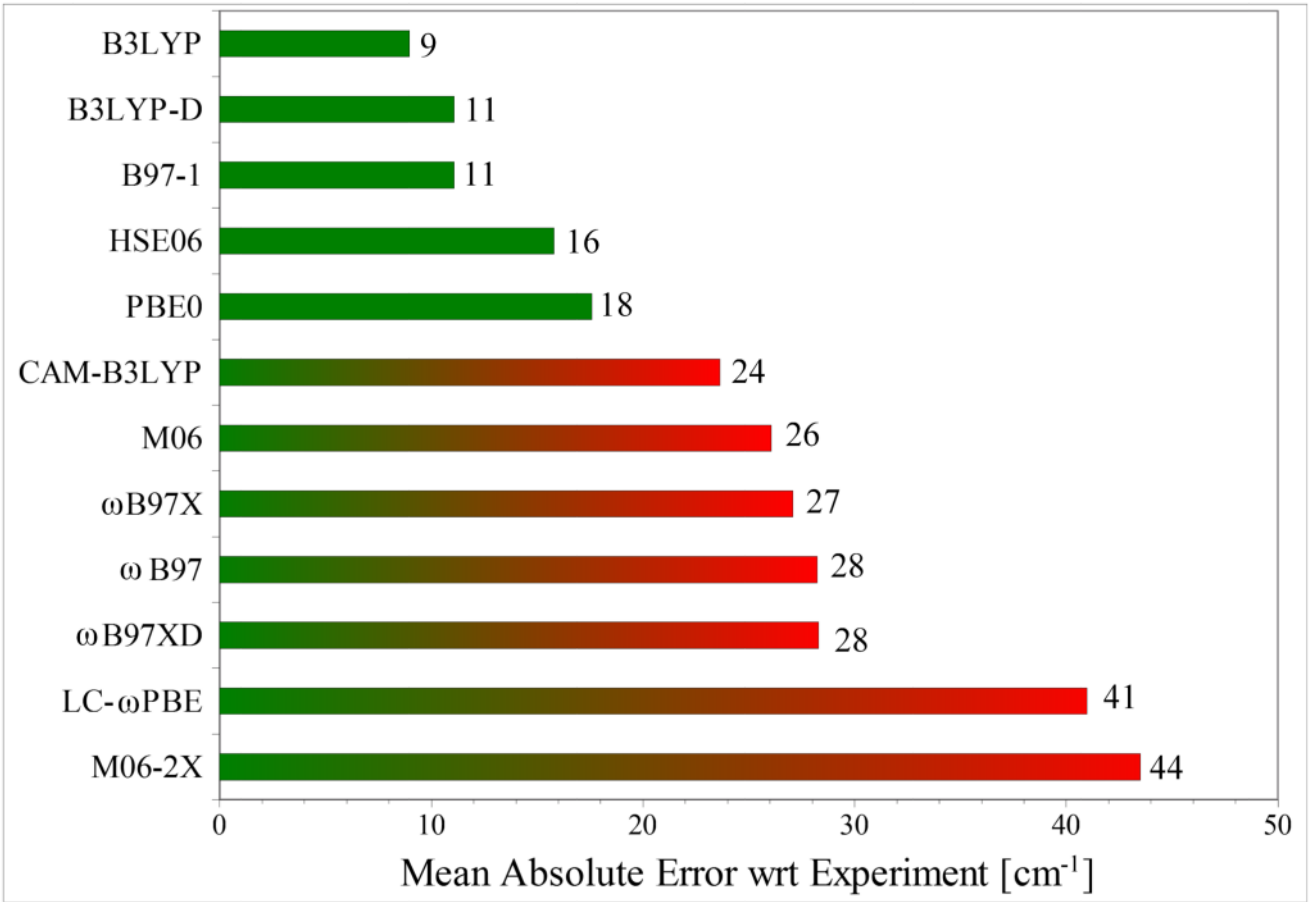

Fig. 1.

Performance of selected hybrid, (B3LYP[134], B97-1[141], PBE0[136], M06[138,139], HSE06[140]), long-range corrected (CAM-B3LYP[135], LC-ωPBE[137], ωB97[142]), and meta-hybrid (M06-2X[138,139]) DFT functionals, including also their dispersion-corrected DFT-D counterparts[143,144] for the computation of anharmonic vibrational wavenumbers at the GVPT2 level. Mean Absolute Error (MAE) with respect to experimental data for a set of small-to-medium-sized molecules from this work (H_2O, NH_3, ethylene, methanol, formaldehyde, F_2CN, H_2CNH, benzene) and as reported in references: adenine[117], anisole[85], furan[85], glycine[83,99,147,151], phenol[85], pyrimidine[83,91], pyridine[85], pyrrole[85], uracil[83,85,92], thiophene[85]. All computations have been performed with basis sets of at least double-ζ plus polarization quality, mainly the SNSD/N07D family (see ESI† for basis set definition): N07D (Ref.[85]), aug-N07D (Refs.[83,91,92,99,151]), SNSD (Ref.[147] and this work), 6-311+G(d,p) (Ref.[219]) and 6-311++G(df,pd) (Ref.[117]).

Europe PMC Funders Author Manuscripts

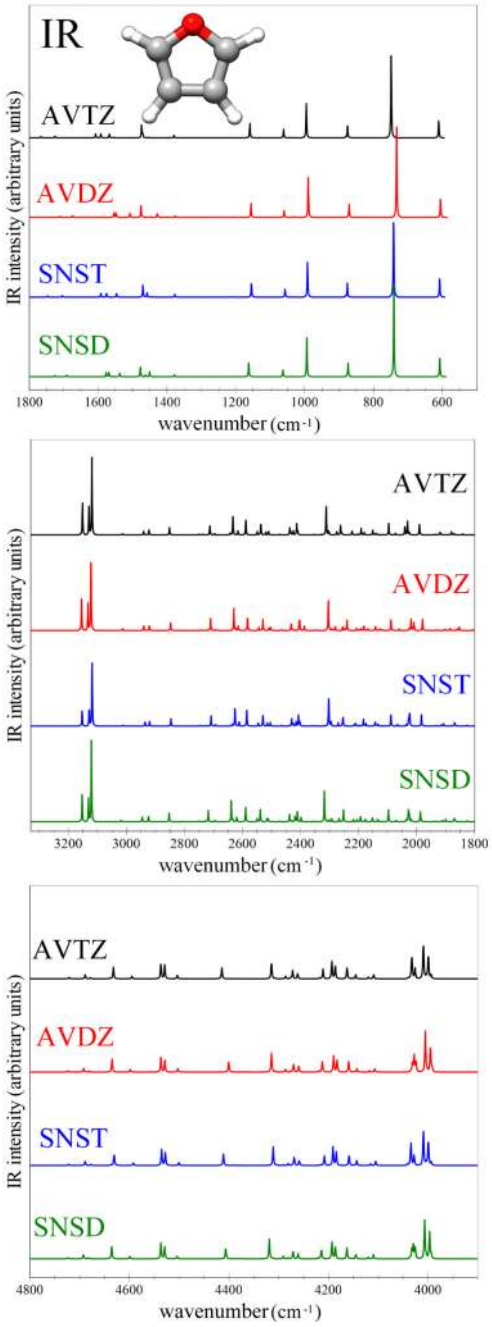

Fig. 2.

Anharmonic IR spectra of furan in the 500–1800 cm^{-1}(upper panel), 1800–3300 cm^{-1}(central panel) and 3900–4800 cm^{-1}(lower panel) wavenumber ranges computed at the B3LYP level with the aug-cc-pVTZ, aug-cc-pVDZ, SNST and SNSD basis sets. Spectra line-shapes have been convoluted with Lorentzian distribution functions with a HWHM of 1 cm^{-1}.

Europe PMC Funders Author Manuscripts

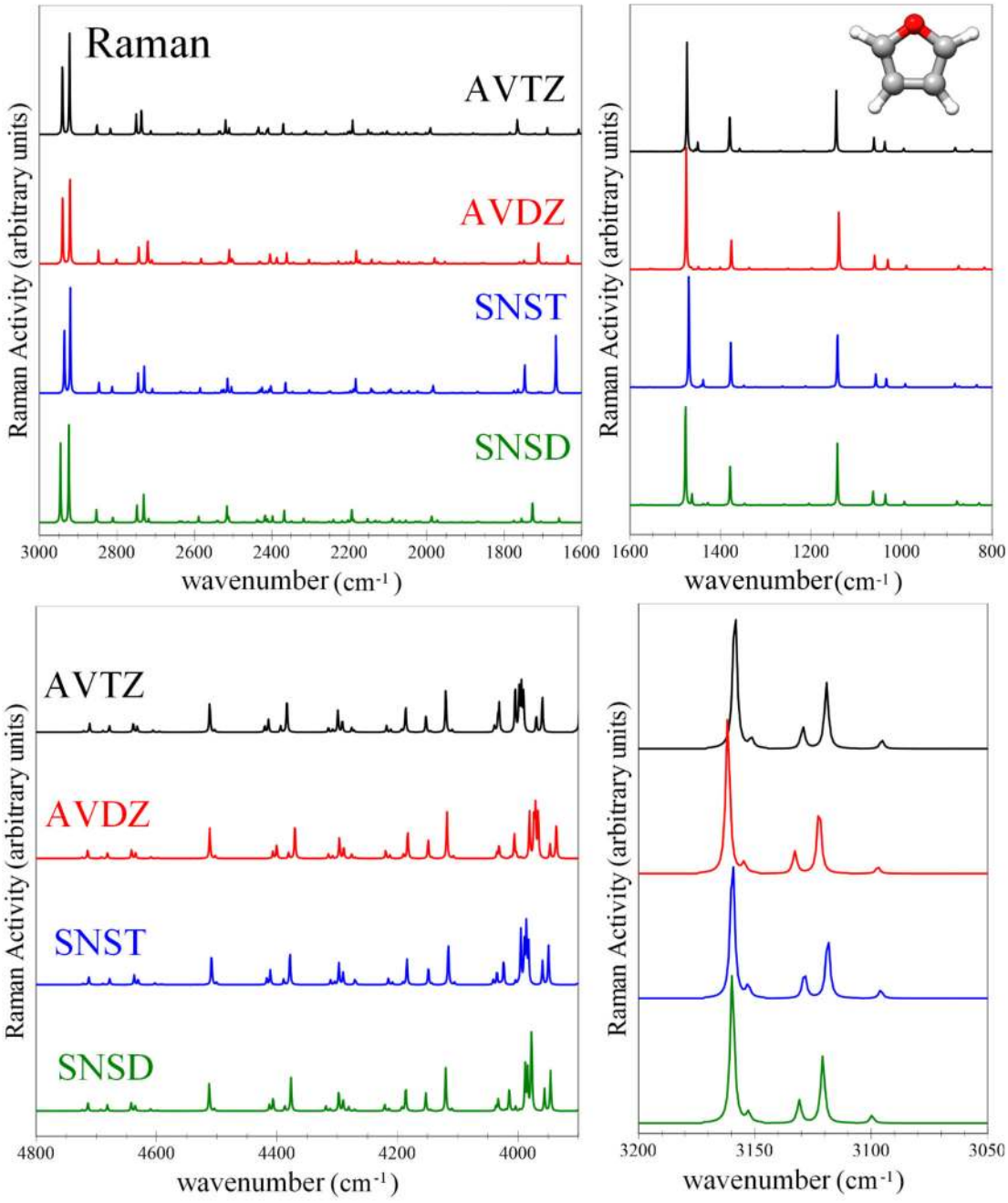

Fig. 3.

Anharmonic Raman spectra of furan in the 800–3000 cm^{-1} 3050–3200 cm^{-1} and 3900–4800 cm^{-1}(lower panel) wavenumber ranges computed at the B3LYP level with the aug-cc-pVTZ, aug-cc-pVDZ, SNST and SNSD basis sets. Spectra line-shapes have been convoluted with Lorentzian distribution functions with a HWHM of 1 cm^{-1}.

Europe PMC Funders Author Manuscripts

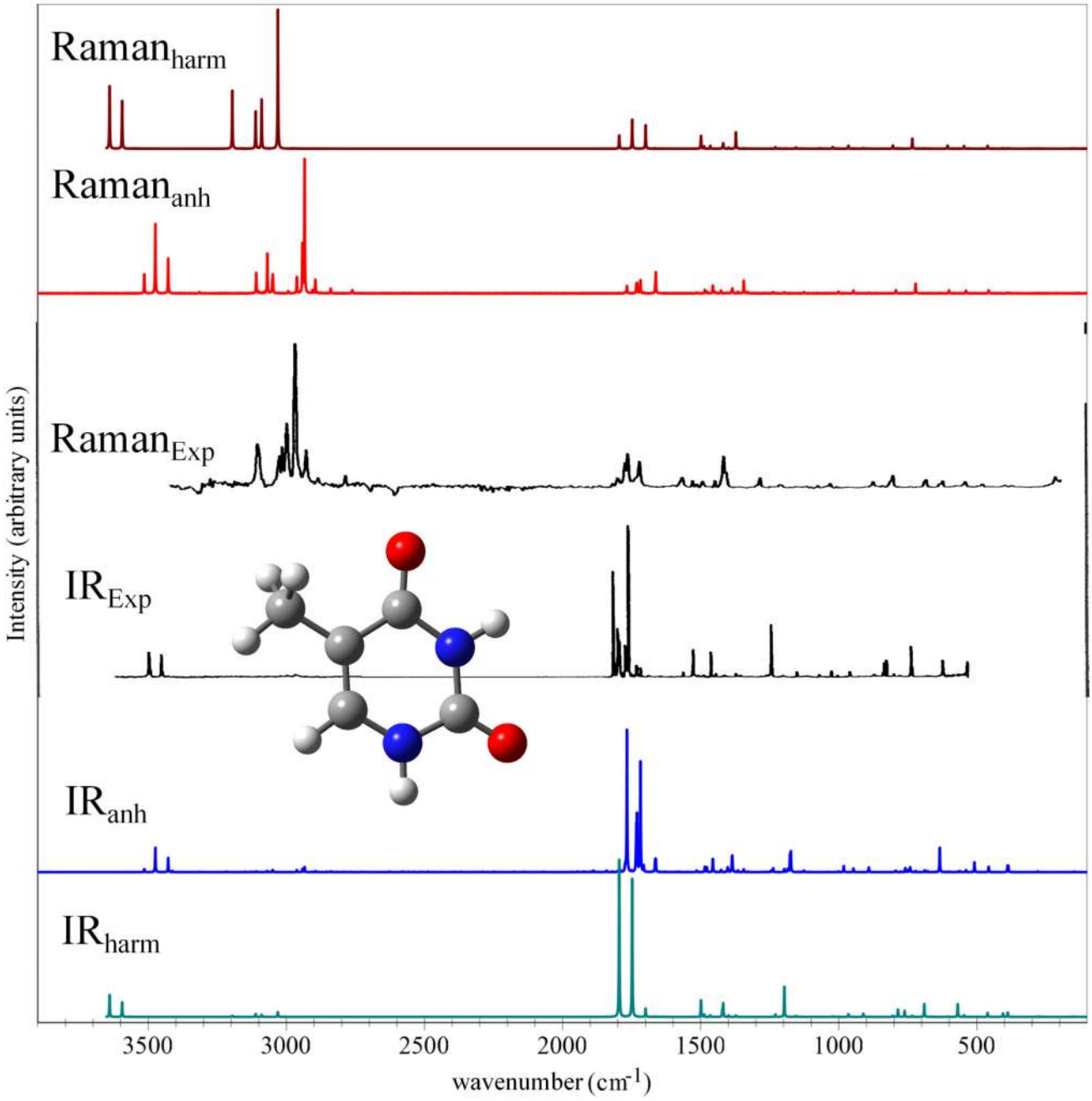

Fig. 4.

Computed anharmonic and experimental IR and Raman[173] spectra of thymine in the 3900–100 cm^{-1} wavenumber range. Theoretical spectra line-shapes have been convoluted with Lorentzian distribution functions with a HWHM of 1 cm^{-1}.

Europe PMC Funders Author Manuscripts

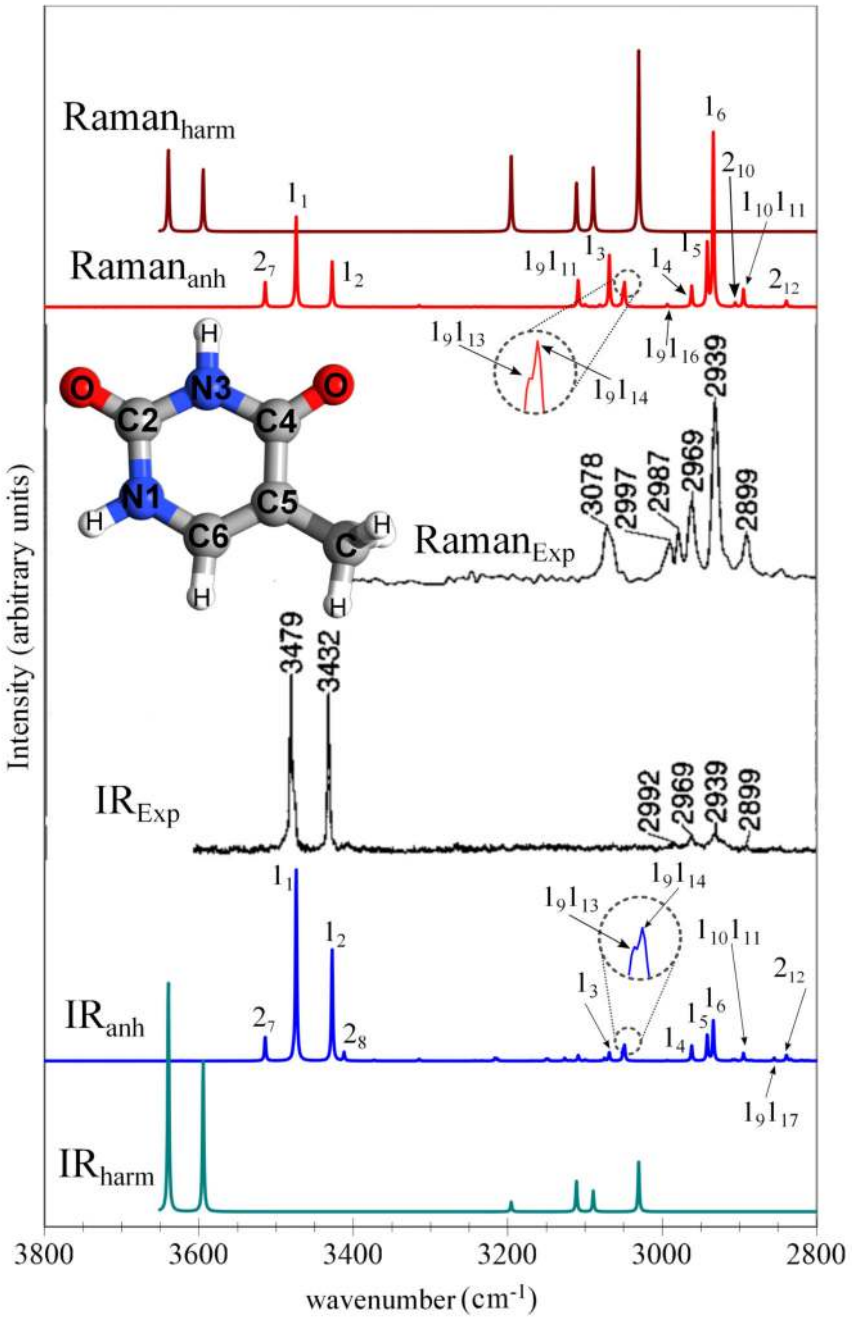

Fig. 5.

Computed anharmonic and experimental IR and Raman[173] spectra of thymine in the 3800–2800 cm^{-1} wavenumber range, along with the assignment of fundamental transitions and most pronounced overtones and combination bands. Theoretical spectra line-shapes have been convoluted with Lorentzian distribution functions with a HWHM of 1 cm^{-1}.

Europe PMC Funders Author Manuscripts

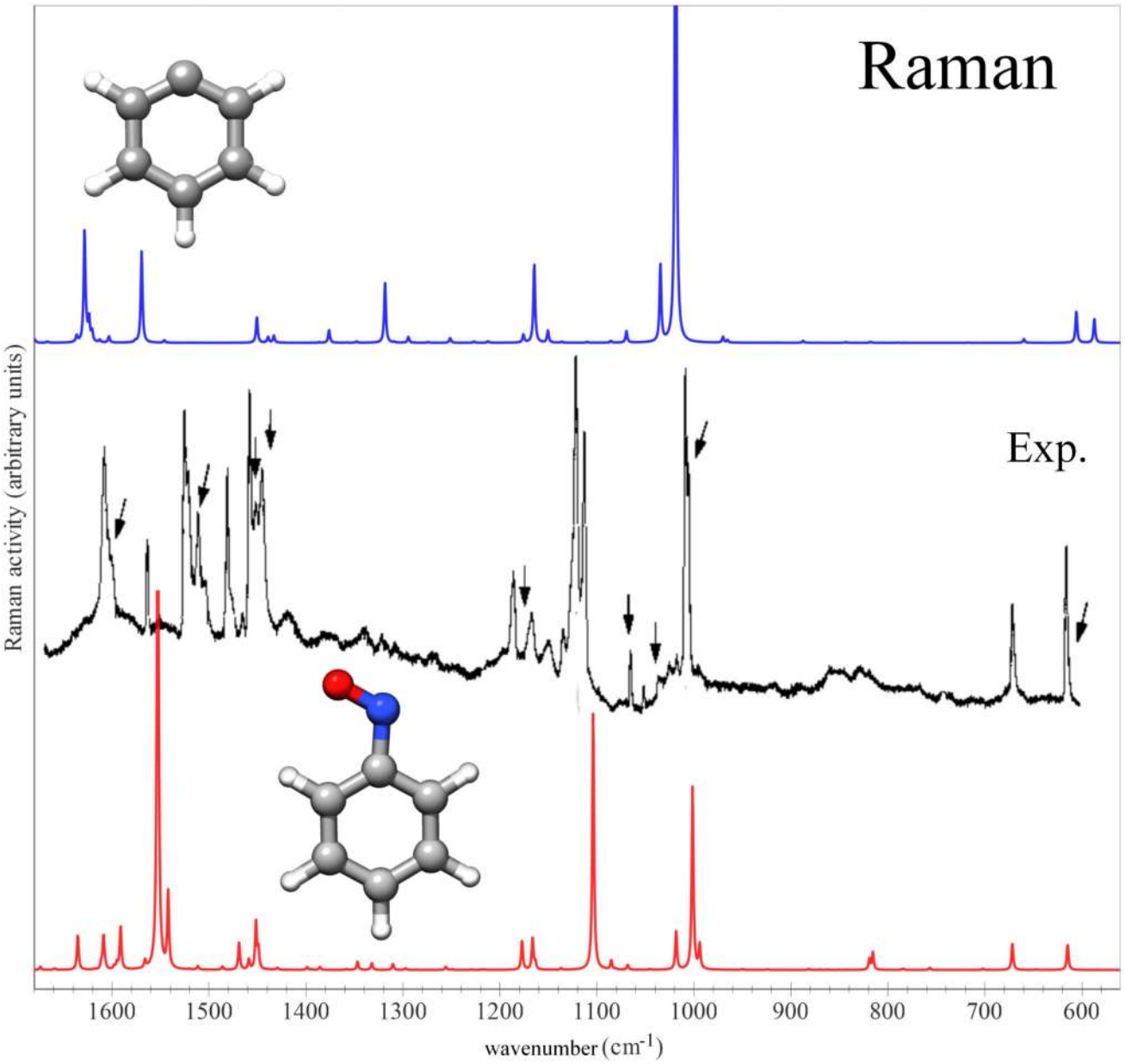

Fig. 6.

Computed anharmonic Raman spectra of the phenyl radical and nitrosobenzene in the 1600–600 cm^{-1} wavenumber range, compared to the experimental Raman[182] spectrum measured in Ar Matrix and obtained after prolonged excimer laser irradiation at 308 nm of nitrosobenzene isolated in Ar matrix at 6 K, with peaks assigned to the C_6H_5 marked by arrows. Theoretical spectra of the phenyl radical and nitrosobenzene from Ref.[153] and this work (B3LYP/SNSD), respectively. Theoretical spectra line-shapes have been convoluted with Lorentzian distribution functions with a HWHM of 1 cm^{-1}.

Europe PMC Funders Author Manuscripts

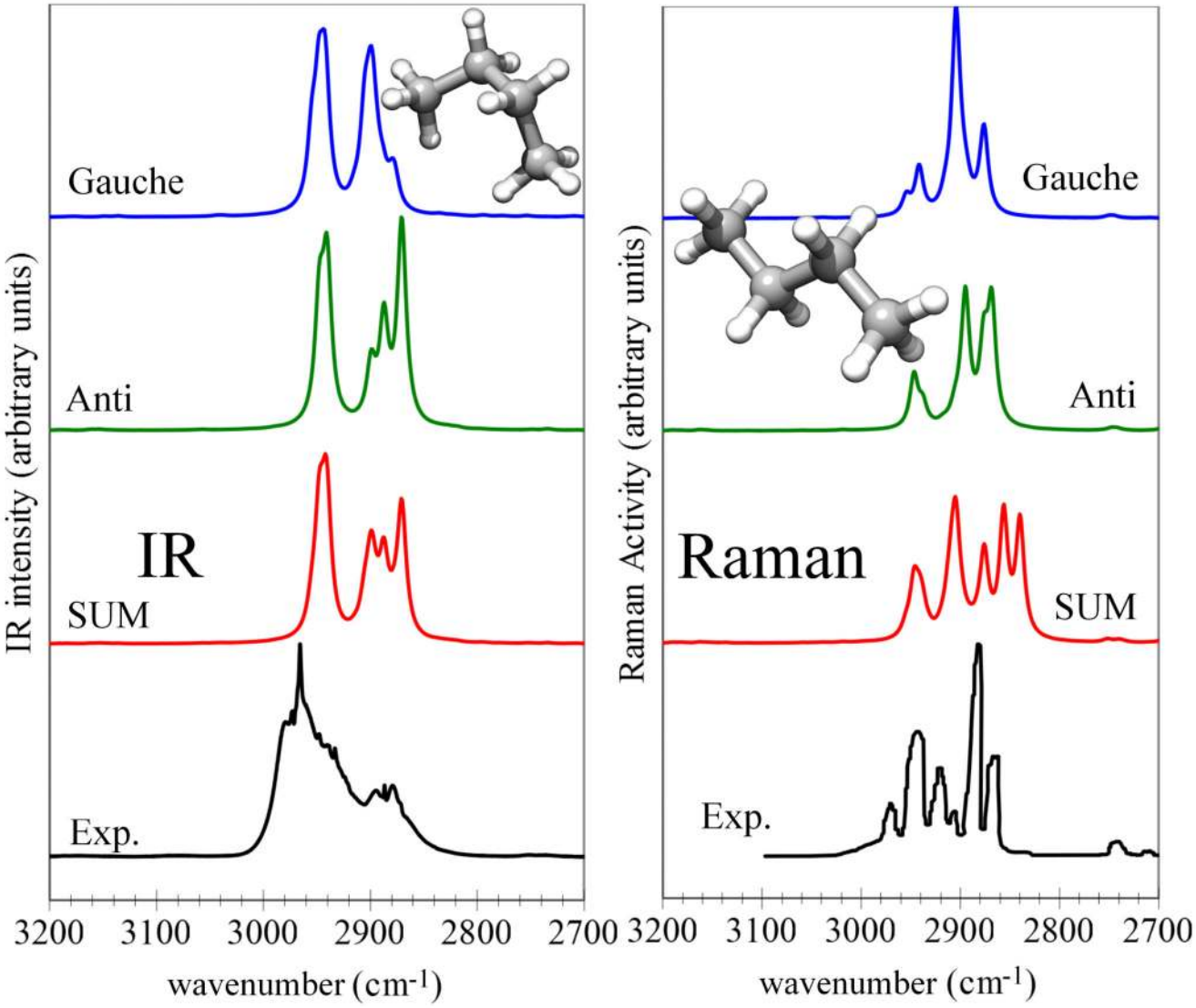

Fig. 7.

Computed anharmonic and experimental IR[192] and Raman[193] spectra of butane in the 3200–2700 cm^{-1} wavenumber range. The theoretical spectra of each conformer, *anti* and *gauche*, and the sum of their contribution weighted by their relative abundances (as computed in this work, T=298K) are presented here. The line-shapes have been convoluted with Lorentzian distribution functions with a HWHM of 5 cm^{-1}.

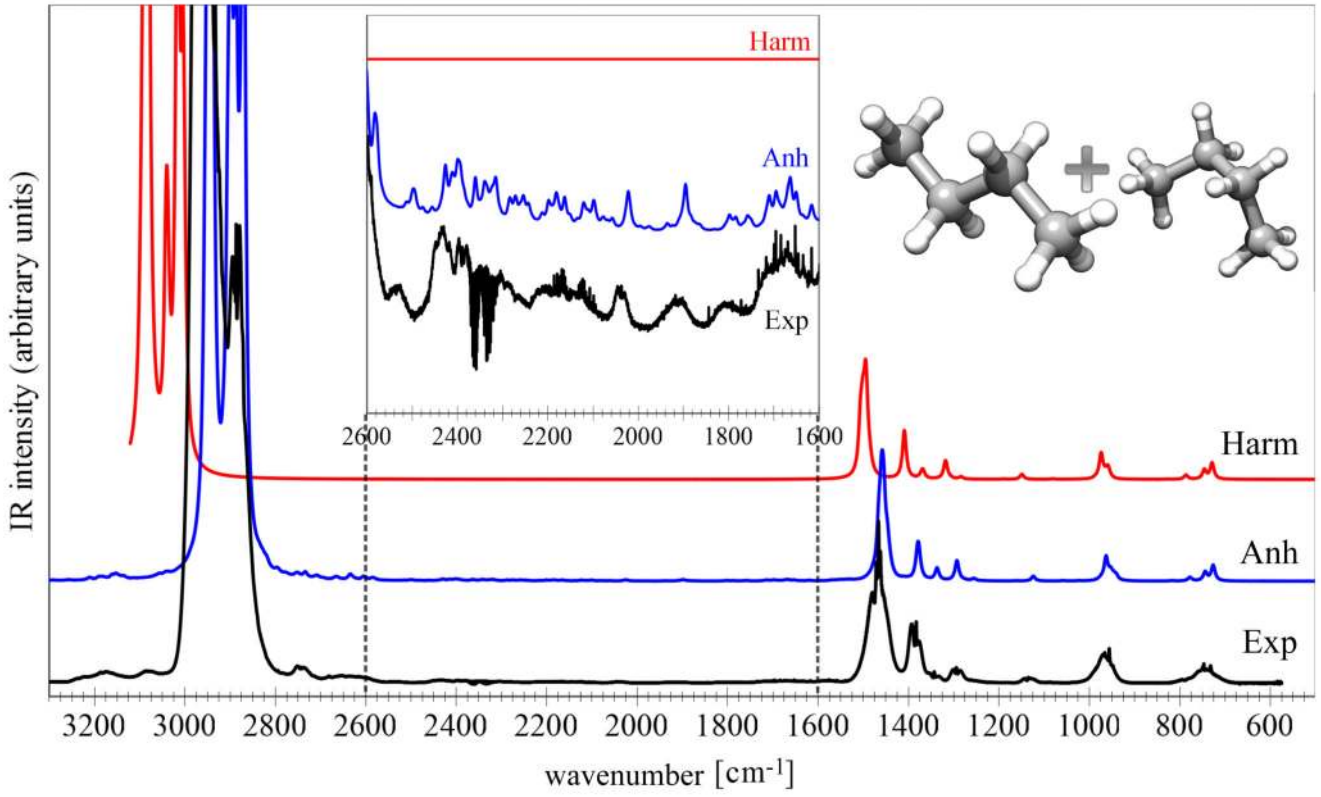

Fig. 8.

Computed harmonic and anharmonic IR spectra of butane in the 3200–600 cm^{-1} wavenumber range compared to experiment[192]. The theoretical spectra of *anti* and *gauche* conformers, the sum of their contribution weighted by their relative abundances (as computed in this work, T=298K) are presented here. The inset shows the 2600–1600 cm^{-1} spectra range fully related to the overtones and combination transitions. Theoretical spectra line-shapes have been convoluted with Lorentzian distribution functions with a HWHM of 5 cm^{-1}.

Europe PMC Funders Author Manuscripts

Europe PMC Funders Author Manuscripts

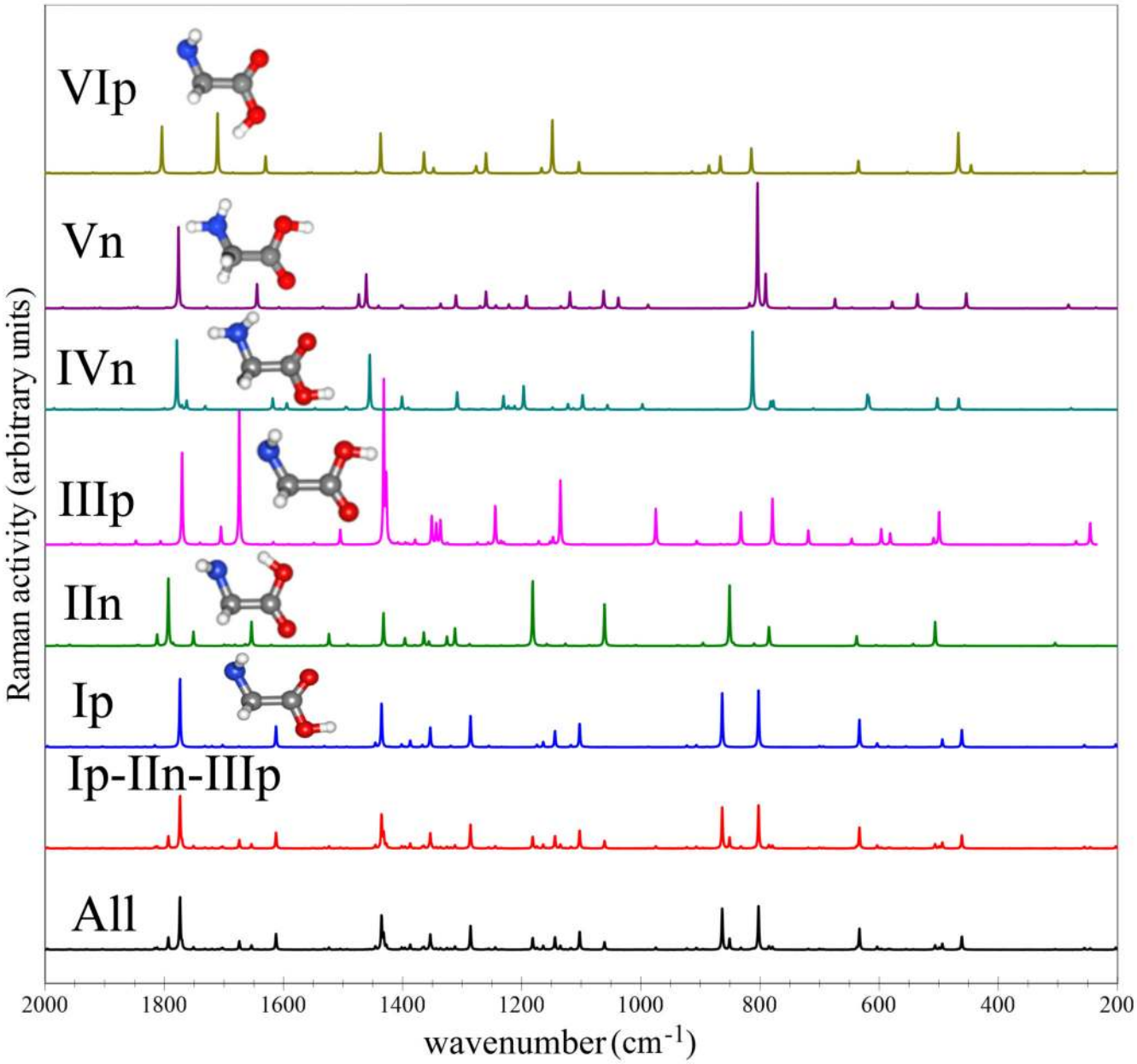

Fig. 9.

Best-estimated Raman spectra in the (2000–200 cm^{-1}) wavenumber region, for the main glycine isotopologue. Simulated theoretical spectra: single spectra for Ip/ttt, IIn/ccc, IIIp/tct, IVn/gtt, Vn/gct and VIp/ttc, the sum of the Ip/ttt, IIn/ccc and IIIp/tct (Ip-IIn-IIIp) contributions weighted by their relative abundances (as computed at the HRAO level at T=410 K[93]), also assuming the conformational cooling IVn/gtt→Ip/ttt and Vn/gct→IIIp/tct), and the Ip-IIn-IIIp sum complemented by minor contributions (1%) from the IVn/gtt, Vn/gct and VIp/tcc (*ALL*). Spectra line-shapes have been convoluted with Lorentzian distribution functions with a half-width at half-maximum (HWHM) of 1 cm^{-1}.

Europe PMC Funders Author Manuscripts

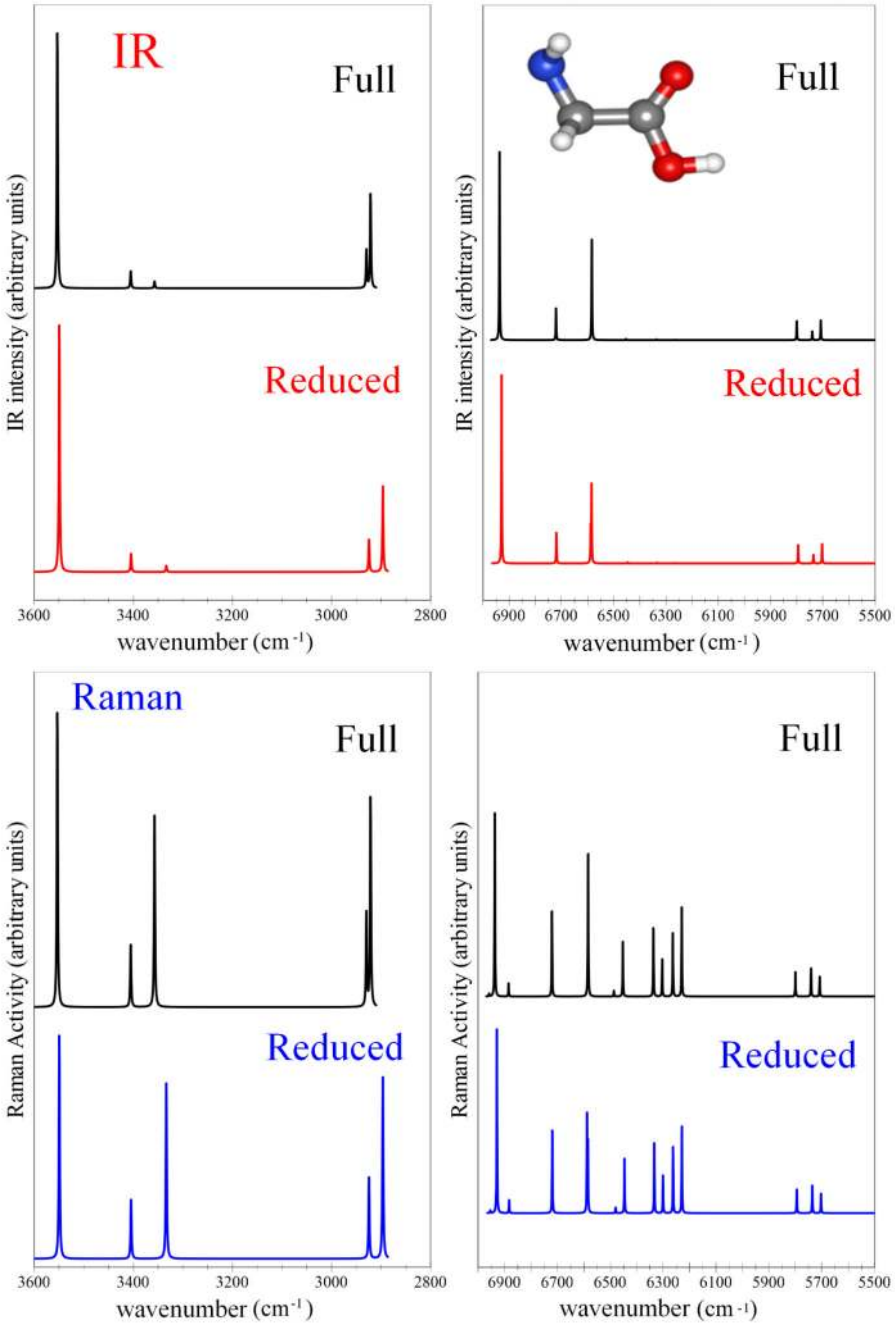

Fig. 10.

Infrared and Raman spectra of the most stable glycine conformer (Ip) in the wavenumber range related to the X-H stretching fundamental transitions (3600–2800 cm^{-1}) and their overtones and combination bands (7000–5500 cm^{-1}). VPT2 computations taking into account all normal modes (Full) and with the reduced dimensionality scheme (Reduced), for the latter all five X-H stretching vibrations have been considered together along with additional inclusion of mode υ_{10}. Spectra line-shapes have been convoluted with Lorentzian distribution functions with a half-width at half-maximum (HWHM) of 1 cm^{-1}.

Europe PMC Funders Author Manuscripts

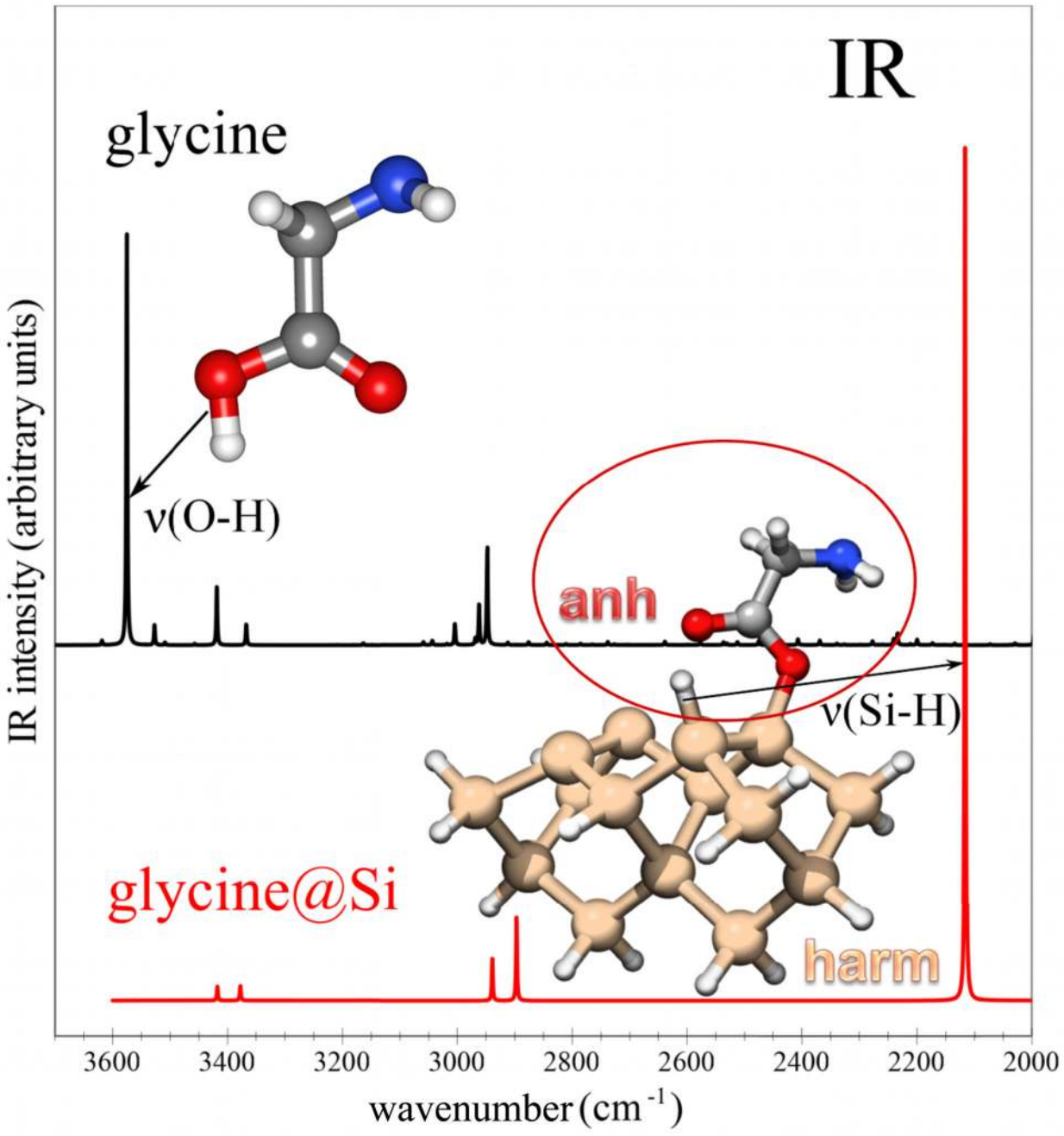

Fig. 11.

Infrared spectra in the wavenumber range related to the X-H stretching fundamental transitions (3600–2000 cm^{-1}) of the most stable glycine conformer (Ip) and glycine adsorbed on the Silicon cluster. In both cases all normal modes of glycine have been included into the GVPT2 computations. Spectra line-shapes have been convoluted with Lorentzian distribution functions with a half-width at half-maximum (HWHM) of 1 cm^{-1}.

Europe PMC Funders Author Manuscripts

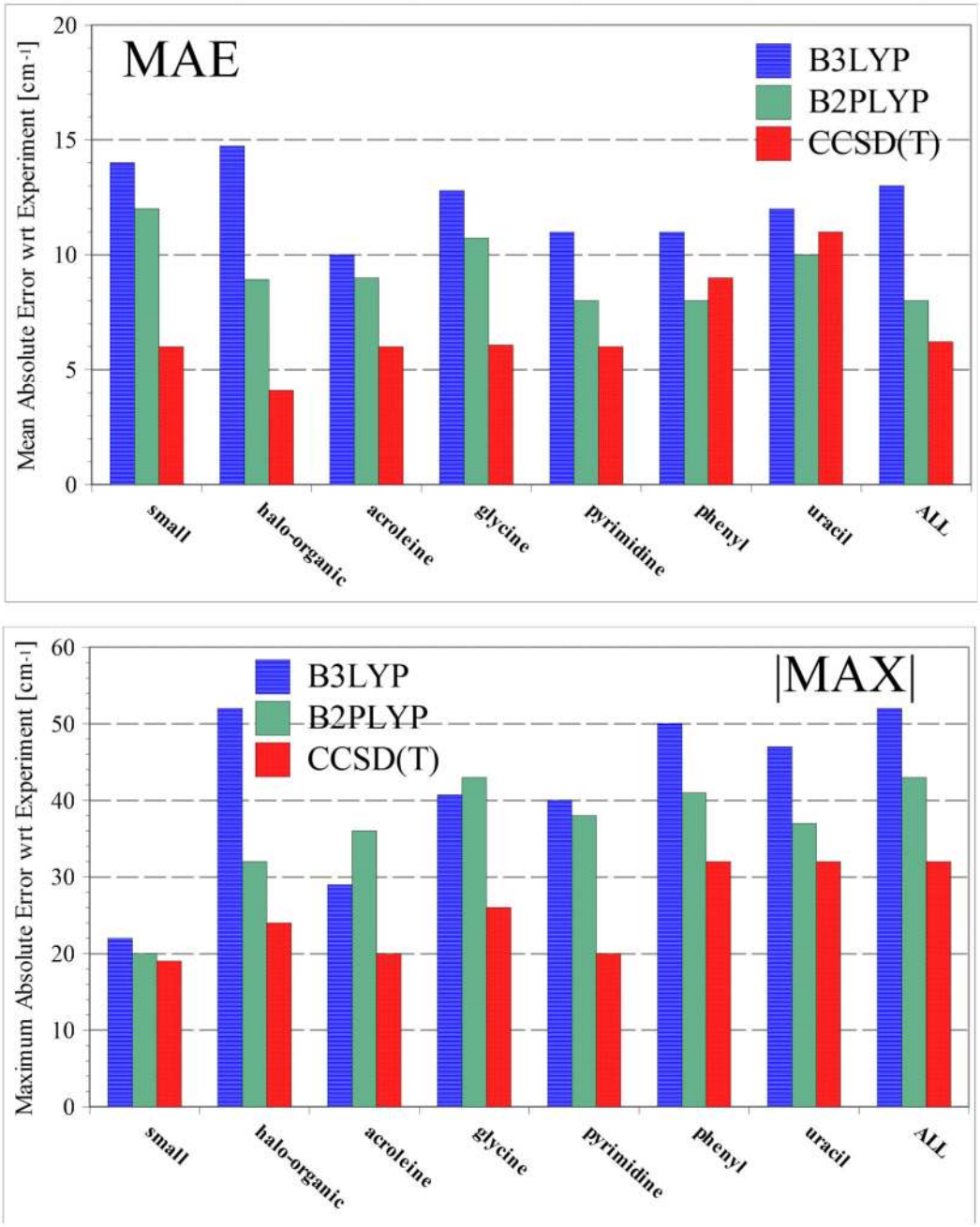

Fig. 12.

Performance of the B3LYP/SNSD and hybrid B2PLYP/B3LYP and CCSD(T)/B3LYP models for the computation of anharmonic vibrational wavenumbers at the GVPT2 level. All anharmonic corrections have been computed at the B3LYP level with basis sets of at least double-ζ plus polarization quality (mainly SNSD/N07D family). For B2PLYP and CCSD(T) harmonic wavenumbers have been computed with basis sets of at least cc-pVTZ quality. Mean Absolute Error (MAE, upper panel) and Maximum Absolute Error (|MAX|, lower panel) with respect to experimental data for about 250 fundamental wavenumbers for

small-to-medium molecular systems as reported in references: small molecules (H_2O, NH_2, NH_3)[83], halo-organic (halo-methanes, halo-ethylenes)[160], acroleine[83], glycine (Ip, IIn, IIIp and VIp conformers)[83,93,99,147,151], phenyl[153], pyrimidine[83,91], uracil[83,85,92], and from this work. Normal modes showing larger deviation for anharmonic correction between B3LYP and B2PLYP and/or CCSD(T) (υ_2 of NH_3 and υ_3 of glycine IIn) have been excluded from statistic (see text).

Europe PMC Funders Author Manuscripts

Europe PMC Funders Author Manuscripts

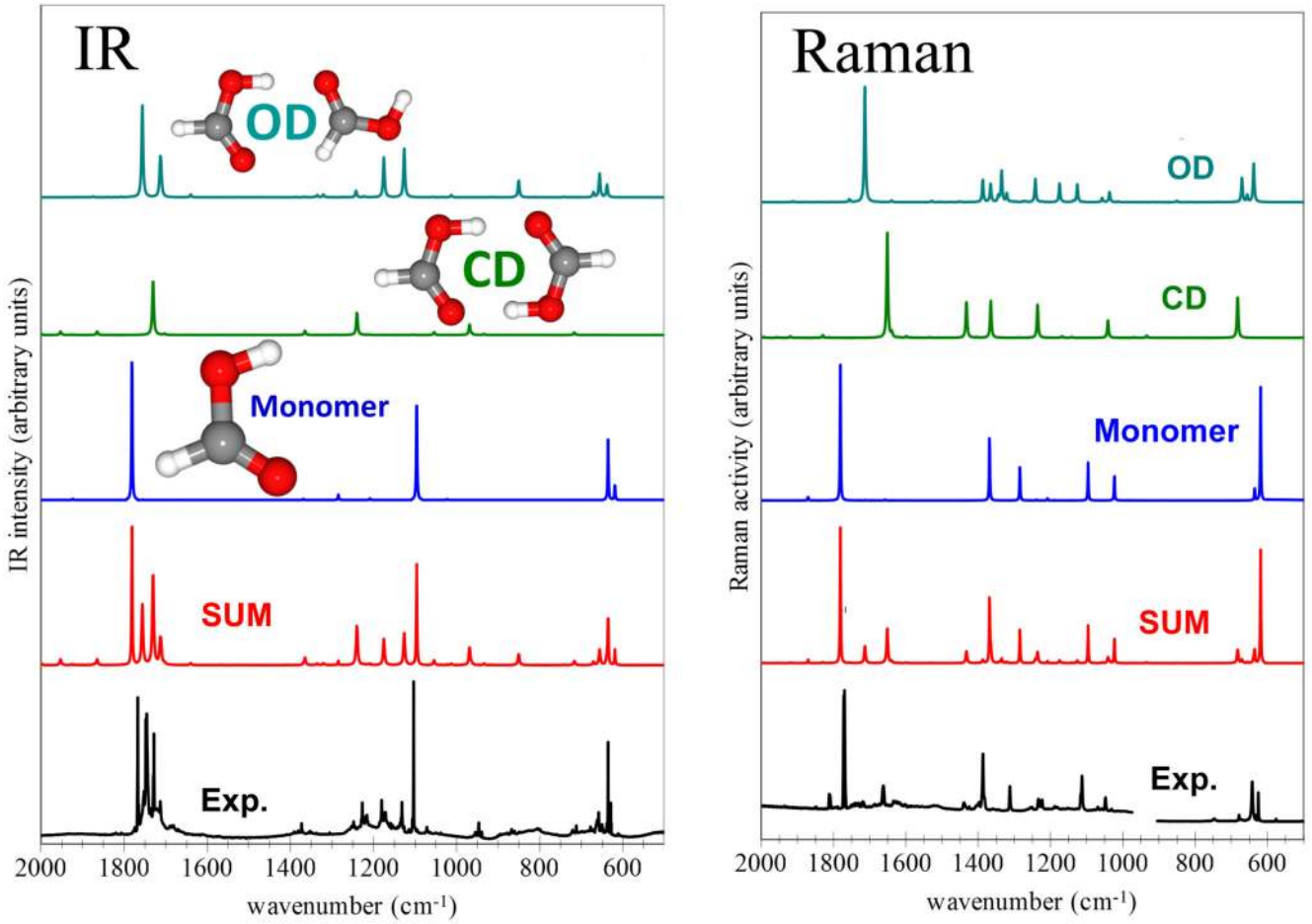

Fig. 13.

Computed anharmonic and experimental IR and Raman[215] spectra of formic acid in the 2000–500 cm^{-1} wavenumber range. For theoretical spectra single contributions from the FA monomer (M) and its most stable dimers, cyclic dimer (CD) and open dimer (OD), and the overall spectra (SUM) obtained as the spectrum of the monomer complemented by the contributions (5-30%) from the CD and CO dimers are presented. Theoretical spectra line-shape of monomer and dimers have been convoluted with Lorentzian distribution functions with HWHMs of 1 cm^{-1} and 2 cm^{-1}, respectively.

Table 1

Wavenumbers (in cm^{-1}), Infrared intensities (in km mol^{-1}) and Raman activities (in $Å^4$ u^{-1}) computed for a set of bi-hetero-atomic closed- and open-shell molecules. All computations at DFT level with B3LYP functional in conjunction with aug-cc-pVXZ (X=D,T,Q) and SNSX (X=D,T) basis sets

Molecule	Basis	Wavenumbers			IR Intensities			Raman Activities		
	set	harm	anh	Δ_{anh}	harm	anh	Δ_{anh}	harm	anh	Δ_{anh}
CH^+	AVQZ	2797.3	2687.2	−110.2	1.3	1.9	0.7	62.9	69.7	6.7
	AVTZ	2793.1	2686.7	−106.4	1.3	1.9	0.6	63.5	70.9	7.4
	AVDZ	2786.7	2677.0	−109.7	1.7	2.5	0.8	67.0	72.4	5.4
	SNST	2809.9	2696.2	−113.7	1.4	2.0	0.6	64.8	71.3	6.5
	SNSD	2807.5	2696.5	−111.0	1.2	1.7	0.5	64.6	71.3	6.8
CN	AVQZ	2153.1	2127.3	−25.8	19.9	19.1	−0.8	205.1	258.1	53.0
	AVTZ	2150.9	2125.1	−25.8	19.7	18.9	−0.8	207.5	262.5	55.1
	AVDZ	2137.6	2112.1	−25.4	18.0	17.2	−0.8	224.5	293.0	68.5
	SNST	2153.4	2127.5	−25.9	20.0	19.1	−0.8	203.2	255.6	52.4
	SNSD	2149.8	2123.9	−25.9	17.1	16.3	−0.8	221.2	283.1	61.9
CO	AVQZ	2212.6	2187.6	−24.9	79.7	79.4	−0.3	17.7	18.1	0.4
	AVTZ	2207.7	2183.0	−24.7	79.9	79.6	−0.3	17.6	18.0	0.4
	AVDZ	2185.7	2161.2	−24.5	78.7	78.3	−0.3	17.0	17.3	0.4
	SNST	2207.6	2182.7	−24.9	81.7	81.3	−0.4	17.1	17.4	0.4
	SNSD	2209.1	2183.6	−25.5	83.4	83.0	−0.4	17.9	18.3	0.4
HF	AVQZ	4078.4	3905.3	−173.1	111.0	108.6	−2.4	39.5	43.6	4.2
	AVTZ	4072.1	3901.0	−171.1	111.4	108.9	−2.5	38.9	43.0	4.1
	AVDZ	4062.0	3871.0	−191.0	111.3	109.4	−1.9	38.6	42.9	4.3
	SNST	4051.9	3876.8	−175.1	112.7	109.7	−3.0	34.4	38.4	4.0
	SNSD	4067.5	3892.0	−175.5	109.6	107.3	−2.3	39.3	43.6	4.2
NH	AVQZ	3263.3	3118.8	−144.5	20.5	22.8	2.2	94.1	103.4	9.3
	AVTZ	3259.6	3117.2	−142.4	20.8	23.2	2.3	93.7	98.7	5.0
	AVDZ	3234.5	3093.5	−141.0	22.3	24.4	2.1	94.3	103.1	8.8
	SNST	3260.3	3115.8	−144.5	21.0	23.3	2.4	94.5	105.5	11.1
	SNSD	3261.8	3120.3	−141.5	22.9	25.5	2.5	94.8	103.7	8.9
NO	AVQZ	1973.5	1948.8	−24.7	42.3	41.9	−0.4	8.5	8.8	0.3
	AVTZ	1968.3	1943.4	−24.9	42.7	42.2	−0.4	9.3	9.5	0.3
	AVDZ	1974.7	1949.6	−25.1	41.8	42.4	0.6	10.2	10.2	0.1
	SNST	1972.3	1946.9	−25.4	42.1	41.6	−0.4	8.9	9.2	0.2
	SNSD	1982.8	1957.3	−25.5	43.3	42.8	−0.5	9.4	9.7	0.3
OH	AVQZ	3701.0	3555.9	−145.1	13.5	12.0	−1.5	61.3	71.1	9.9
	AVTZ	3693.1	3543.4	−149.7	13.3	12.0	−1.3	60.8	67.0	6.2

Europe PMC Funders Author Manuscripts

Molecule	Basis	Wavenumbers			IR Intensities			Raman Activities		
	set	harm	anh	Δ_{anh}	harm	anh	Δ_{anh}	harm	anh	Δ_{anh}
	AVDZ	3681.8	3528.8	−153.0	12.8	11.6	−1.2	60.6	66.7	6.1
	SNST	3693.0	3542.1	−150.9	13.7	12.2	−1.5	60.3	66.4	6.1
	SNSD	3705.5	3554.4	−151.1	12.6	11.2	−1.4	60.8	67.0	6.2

Table 2

Harmonic and anharmonic vibrational wavenumbers (in cm^{-1}), IR intensities (in km mol^{-1}) and Raman activities (in $Å^4$ u^{-1}) computed for the benchmark set composed of small closed- and open-shell molecules (CH^+, CN, CO, HF, NH, NO, OH, H_2O, H_2CO, H_2CN, C_2H_4, CH_2F_2, CH_3NH_2, CH_3OH, CHOOH). All computations were done at the DFT level with the B3LYP functional in conjunction with the aug-cc-pVXZ (X=D,T,Q) and SNSX (X=D,T) basis sets. Mean absolute errors (MAE) and maximum absolute errors |MAX| are reported with respect to the B3LYP/aug-cc-pVQZ results[a]

Basis	Wavenumbers			IR Intensities			Raman Activities		
set	harm	anh	Δ_{anh}	harm	anh	Δ_{anh}	harm	anh	Δ_{anh}
	MAE								
AVTZ	2.3	2.3	1.0	0.2	0.2	0.1	0.2	0.6	0.5
AVDZ	13.8	13.3	4.2	1.1	1.1	0.3	0.8	1.3	0.7
SNST	5.0	4.7	1.2	0.5	0.5	0.2	0.4	0.6	0.3
SNSD	7.0	6.5	1.6	0.8	0.8	0.2	0.6	1.0	0.5
	|MAX|								
AVTZ	7.9	12.4	13.4	0.9	1.1	0.5	2.4	4.7	4.3
AVDZ	33.0	34.3	17.9	6.0	5.8	4.8	19.4	34.9	15.5
SNST	29.6	28.5	5.8	2.4	3.9	1.8	5.1	5.2	3.8
SNSD	22.4	22.6	8.2	5.9	5.1	3.8	16.1	25.0	8.9

[a] modes showing strong Fermi interactions (υ_5 of H_2CO; υ_9 of C_2H_4, υ_1 and υ_2 of CH_2F_2; υ_3, υ_4 and υ_5 of CH_3NH_2; υ_3, υ_4 and υ_5 of CH_3OH;) have been excluded from statistics.

Table 3

Harmonic and anharmonic vibrational wavenumbers (in cm^{-1}), IR intensities (in km mol^{-1}) and Raman activities (in $Å^4$ u^{-1}) computed for the benchmark set composed of medium-size closed- and open-shell molecules (furan, pyrrole, pyrimidine, glycine, phenyl). All computations were done at the DFT level with the B3LYP functional in conjunction with the aug-cc-pVXZ (X=D,T) and SNSX (X=D,T) basis sets. Mean absolute errors (MAE) and maximum absolute errors |MAX| are reported with respect to the B3LYP/aug-cc-pVTZ results[a]

Molecule	Basis	Wavenumbers			IR Intensities			Raman Activities		
	set	harm	anh	Δ_{anh}	harm	anh	Δ_{anh}	harm	anh	Δ_{anh}
		MAE								
furan	AVDZ	9.6	8.5	2.8	2.0	2.2	0.4	1.5	1.8	0.7
	SNST	3.4	3.5	1.5	0.3	0.4	0.2	0.9	1.1	0.6
	SNSD	4.9	4.7	1.9	2.1	2.1	0.4	1.0	0.9	1.0
pyrrole	AVDZ	8.6	9.1	4.6	1.0	1.4	0.9	1.2	1.7	1.0
	SNST	3.7	5.6	2.7	0.4	0.9	0.7	0.4	1.3	1.1
	SNSD	5.0	6.5	2.5	0.7	0.6	0.5	0.7	0.9	0.7
pyrimidine	AVDZ	7.4	7.6	4.1	1.0	1.5	0.6	1.1	2.1	1.4
	SNST	2.2	5.2	3.9	0.3	0.7	0.5	0.4	1.3	1.5
	SNSD	4.7	5.9	3.0	0.9	1.1	0.5	0.7	1.1	0.8
glycine	AVDZ	6.7	8.4	4.4	1.9	4.8	4.1	0.3	1.6	1.3
	SNST	2.9	4.0	2.6	1.9	3.5	2.8	0.3	1.1	1.0
	SNSD	3.6	5.8	4.1	4.2	3.6	3.9	0.4	0.7	0.6
phenyl	AVDZ	8.1	9.4	8.1	0.3	1.9	2.0	1.6	2.4	1.4
	SNST	1.5	5.6	4.8	0.2	1.6	1.7	1.3	2.6	2.5
	SNSD	4.4	6.1	4.4	0.3	0.3	0.3	2.3	3.1	1.9
ALL	AVDZ	8.0	8.6	4.8	1.2	2.4	1.6	1.1	1.9	1.2
	SNST	2.7	4.8	3.1	0.6	1.5	1.2	0.6	1.5	1.3
	SNSD	4.5	5.8	3.2	1.6	1.5	1.1	1.0	1.4	1.0
		|MAX|								
furan	AVDZ	28.9	27.4	9.1	15.9	16.7	2.6	8.0	13.9	5.9
	SNST	8.4	10.1	4.5	1.3	1.4	1.2	5.8	6.5	4.7
	SNSD	15.9	15.4	8.3	15.9	16.7	2.2	4.9	6.7	7.9
pyrrole	AVDZ	23.1	28.2	22.5	9.8	11.5	11.2	6.8	11.9	5.8
	SNST	11.0	19.7	11.3	4.8	4.9	4.2	2.4	13.4	12.9
	SNSD	15.9	28.2	23.3	6.1	5.6	1.6	3.3	5.8	3.9
pyrimidine	AVDZ	14.8	20.5	19.4	5.8	5.3	5.5	7.6	20.1	13.7
	SNST	5.5	28.0	25.6	1.5	4.8	3.9	3.4	13.4	12.6
	SNSD	12.6	23.8	20.3	4.3	3.6	3.6	6.3	10.0	4.8
glycine	AVDZ	18.5	31.1	19.7	6.5	37.0	32.0	2.2	17.2	15.0
	SNST	12.4	27.2	22.4	9.8	14.5	21.6	1.4	9.9	10.5
	SNSD	13.2	26.7	27.1	31.7	24.6	25.6	2.4	3.3	5.6

Europe PMC Funders Author Manuscripts

Molecule	Basis	Wavenumbers			IR Intensities			Raman Activities		
	set	harm	anh	Δ_{anh}	harm	anh	Δ_{anh}	harm	anh	Δ_{anh}
phenyl	AVDZ	17.0	35.2	21.9	2.9	37.9	40.8	9.3	20.1	10.8
	SNST	5.5	19.6	15.4	1.9	12.0	13.8	10.4	15.4	17.7
	SNSD	11.8	14.1	13.4	1.5	1.8	3.3	13.8	26.8	13.3
ALL	AVDZ	28.9	35.2	22.5	15.9	37.9	40.8	9.3	20.1	15.0
	SNST	12.4	28.0	25.6	9.8	14.5	21.6	10.4	15.4	17.7
	SNSD	15.9	28.2	27.1	31.7	24.6	25.6	13.8	26.8	13.3

Table 4

Anharmonic vibrational wavenumbers (in cm^{-1}), IR intensities (in km mol^{-1}) and Raman activities (in $Å^4\ u^{-1}$) of thymine in the high-wavenumber region of the Raman/IR spectra, along with the available experimental results.

Exp.[a]			Calc.			State	Assignment
Wn	IR[b]	RA[b]	Wn	IR	RA		
			3514.2	10.9	34.4	2_7	νC_2O
3479	130	n.a.	3474.1	85.7	121.3	1_1	νN_1H
3432	110	n.a.	3427.6	49.4	60.5	1_2	νN_3H
			3412.1	3.8	0	2_8	νC_4O
			3108.9	2.5	35.4	$1_9 1_{11}$	$\nu C_5C_6+\delta_{sciss}CH_2$
3078		74	3068.6	3.7	69.5	1_3	νC_6H
			3050.7	4.1	17.3	$1_9 1_{13}$	$\nu C_5C_6+\delta N_1H+\nu C_2N_3$
			3048.9	6.2	28.7	$1_9 1_{14}$	$\nu C_5C_6+in\nu CH_3$
2997[c]			2993.4	0.2	3.8	$1_9 1_{16}$	$\nu C_5C_6+\delta C_6H$
2987[c]/2992	7	42[d]	2962.0	6.8	27.8	1_4	$\nu_{asym}\ CH_3$
2969	13	55	2941.8	11.9	87.7	1_5	$\nu_{out-of-plane}\ CH_3$
2939	20	162	2933.9	17.8	231.7	1_6	$\nu_{sym}\ CH_3$
			2905.5	0.5	5.5	2_{10}	υ_{10}
2899			2894.8	3.6	24.2	$1_{10} 1_{11}$	$\delta N_1H+\delta_{sciss}CH_3+\nu C_2N_3$
			2855.1	1.4	0.8	$1_9 1_{17}$	$\nu C_5C_6+\nu C_5-CH_3$
			2839.3	1.9	7.8	2_{12}	γCH_3

[a] Experimental data from IR and Raman spectrum recorded in low-temperature Ar Matrix from Ref. [173]

[b] The experimental values for the IR intensity and Raman activity are relative values, see Ref. [173] for the details.

[c] The doublet at 2997 cm^{-1} and 2987 cm^{-1} has been assigned in Ref. [173] to the Fermi resonance between the 14 fundamental and some combination band.

[d] Total relative intensity for all of the sub-bands, see Ref. [173] for the details.

Europe PMC Funders Author Manuscripts

Table 5

Harmonic and anharmonic vibrational wavenumbers (in cm^{-1}) of formic acid computed at different levels of theory. Hybrid B2PLYP/B3LYP scheme: harmonic wavenumbers computed at the B2PLYP/aug-cc-pVTZ level and anharmonic corrections computed by B3LYP with SNSD (anh D) and SNST (anh T) basis sets, respectively.

No.	Sym.	B3LYP/SNSD		B3LYP/SNST		B3LYP/AVTZ		B2PLYP/AVTZ		B2PLYP/B3LYP		Ass.	Exp.	
		harm	anh	harm	anh	harm	anh	harm	anh	anh D	anh T		Gas[a]	Ar[b]
υ_1	A’	3726	3541	3707	3521	3716	3531	3733	3549	3548	3555	ν(O-H)	3569	3553
υ_2	A’	3061	2905	3055	2900	3048	2892	3091	2934	2935	2937	ν(C-H)	2942	2958
υ_3	A’	1814	1781	1811	1778	1811	1778	1795	1760	1761	1761	ν(C=O)	1777	1769
υ_4	A’	1397	1370	1400	1372	1402	1373	1407	1379	1380	1381	σ(C-H)	1381	1382
υ_5	A’	1297	1217	1295	1214	1298	1212	1302	1221	1222	1229	σ(C-O-H)	1223[c]	1218
υ_6	A’	1129	1097	1120	1088	1121	1088	1124	1092	1093	1094	ν(C-O)	1104	1107
υ_7	A’	626	620	630	622	629	622	627	621	621	621	π(O-H)	625	626
υ_8	A”	1043	1023	1046	1026	1052	1032	1056	1035	1036	1036	σ(O-C-O)	1033[c]	1040
υ_9	A”	675	641	672	639	675	638	676	643	643	648	π(C-H)	642	633
MAE[a,d]			12.2		15.3		14.6		7.6	7.1	7.0			
|MAX|[a,d]			37		48		50		20	21	16			
MAE[b,d]			14.9		17.5		16.7		8.8	8.5	9.1			
|MAX|[b,d]			53		58		66		24	21	21			

[a] Experimental data from Raman spectrum recorded in the gas phase from Ref. [217]

[b] Experimental data from Raman spectrum recorded in the low-temperature Ar Matrix from Ref. [215]

[c] Experimental data from IR spectrum recorded in the gas phase from Ref. [218]

[d] Mean absolute errors (MAE) and maximum absolute errors |MAX| with respect to experimental results.

Europe PMC Funders Author Manuscripts

Table 6

Harmonic and anharmonic IR intensities (in km mol^{-1}) of formic acid computed at different levels of theory. Hybrid B2PLYP/B3LYP scheme: harmonic wavenumbers computed at the B2PLYP/aug-cc-pVTZ level and anharmonic corrections computed by B3LYP with SNSD (anh D) and SNST (anh T) basis sets, respectively.

No.	Sym.	B3LYP/SNSD		B3LYP/SNST		B3LYP/AVTZ		B2PLYP/AVTZ		B2PLYP/B3LYP	
		harm	anh	harm	anh	harm	anh	harm	anh	anh D	anh T
υ_1	A’	60.0	49.9	62.7	52.2	60.5	50.8	67.5	57.3	57.0	56.9
υ_2	A’	38.9	41.8	38.4	41.0	39.8	42.3	36.0	37.4	37.6	37.4
υ_3	A’	375.4	355.8	373.4	354.0	373.0	353.6	353.2	333.1	333.8	334.4
υ_4	A’	2.6	2.3	2.7	2.3	2.4	2.2	2.0	1.7	1.7	1.7
υ_5	A’	8.4	10.2	7.5	9.5	9.1	12.1	9.9	11.9	11.6	11.5
υ_6	A’	257.9	256.8	264.9	263.3	262.1	260.1	261.8	260.9	260.9	261.0
υ_7	A’	41.6	38.9	41.3	38.7	41.5	39.1	41.0	38.3	38.2	38.1
υ_8	A”	2.3	2.0	2.3	2.0	2.1	1.7	2.6	2.3	2.3	2.3
υ_9	A”	137.2	134.5	137.8	135.5	137.3	134.8	136.5	133.9	133.8	134.2

Europe PMC Funders Author Manuscripts

Table 7

Harmonic and anharmonic Raman activities (in $Å^4\ u^{-1}$) of formic acid computed at different levels of theory. Hybrid B2PLYP/B3LYP scheme: harmonic wavenumbers computed at the B2PLYP/aug-cc-pVTZ level and anharmonic corrections computed by B3LYP with SNSD (anh D) and SNST (anh T) basis sets, respectively.

No.	Sym	B3LYP/SNSD		B3LYP/SNST		B3LYP/AVTZ		B2PLYP/AVTZ	B2PLYP/B3LYP	
		harm	anh	harm	anh	harm	anh	harm	anh D	anh T
υ_1	A’	75.7	89.9	76.2	90.4	75.2	89.2	71.8	85.3	85.3
υ_2	A’	124.7	136.7	123.1	134.8	122.2	134.2	117.0	123.9	123.5
υ_3	A’	13.8	13.6	13.4	13.2	13.4	13.3	15.0	14.9	14.9
υ_4	A’	4.6	5.3	4.7	5.4	4.6	5.3	5.0	5.7	5.7
υ_5	A’	2.3	2.6	2.2	2.5	2.2	2.5	2.3	2.6	2.6
υ_6	A’	2.5	2.3	2.4	2.2	2.3	2.2	3.1	3.0	3.0
υ_7	A’	3.4	3.8	3.3	3.8	3.3	3.8	3.4	3.9	3.9
υ_8	A”	1.2	1.5	1.0	1.4	1.0	1.4	0.9	1.3	1.3
υ_9	A”	0.4	0.5	0.5	0.6	0.5	0.6	0.4	0.5	0.5